CHAPTER 6

LAMB WAVE SIGNAL PROCESSING

****

In previous chapters, numerical method for the simulation of wave propagation problems is presented. Subsequently, *a posteriori* error estimation technique for wave propagation problems is developed. The third task of the thesis is to develop efficient algorithms for locating damage from the contaminated Lamb wave signals. From this perspective, decomposition of the noisy signal into its constituent components is a critical requirement for accurate damage detection and feature extraction. The chapter is divided into two major sections: one for noise filtering techniques for guided waves in diagnosis of structural cracks in the plate-like structures. The second section is devoted to modeling of Lamb wave for cylindrical structures and selection of optimal noise filtering technique.

The purpose of this chapter is to provide optimal noise filtering technique for Lamb waves in the diagnosis of structural singularities. Although many techniques have been developed over the past several years to suppress random noise in Lamb wave signal, filtration of interferences of wave modes and boundary reflection is not in a much matured stage and thus needs further investigation. The present study contains detailed information about various noise filtering methods, newly developed filtration technique and their efficacy in handling the above mentioned issues. We propose WMFM, a combination of the wavelet transform and matched filtering method, which can significantly improve the accuracy of the filtered signal and identify relatively small damage. Correlation coefficient and RMSE are additionally computed for performance evaluation of the filters

using various Signal to Noise Ratio (SNR). The proposed filtering techniques can be utilized in online monitoring of civil and mechanical structures. The algorithm of the method is easy to implement and found to be successful in accurately detecting damage. The objective of this study is to establish the effectiveness of the multi-feature filtering techniques of signal analysis and assessing the capabilities of Matched Filter Technique MFT and newly developed WMFM method for field application of Lamb wave propagation based SHM system.

6.1 Diagnosis of Structural Cracks in the Plate-Like Structures

6.1.1 Introduction

Lamb wave based nondestructive inspection techniques provides an evaluation of the integrity of structures and to find out damage position, shape, and size (Lee and Staszewski (2003), Staszewski (2004), Farrar and Worden (2007), Croxford *et al.* (2007), Kumar and Hundal (2008), Su and Ye (2009), Park *et al.* (2010)). There are many application areas for Lamb waves such as identification of actual defects on site (Zhao *et al.* (2007)), delaminations of composite (Kessler *et al*. (2002)), adhesive defects on stiffeners (Fan *et al.* (2013)), material characterization and their usage to reveal mechanical properties of plate like structures (Safaeinili *et al.* (1996)). A significant advantage of guided Lamb waves is that a large area can be tested with single excitation and without moving the transducer. Cawley *et al.* (2003) have established that Lamb waves can propagate at relatively long distances with minuscule amplitude decay and are useful for the inspection of the major metallic structures. However, there are various complications which come up in the received Lamb waves signals because of multiple propagation modes with different group velocity in the single frequency and dispersive

behavior of waves as well as the mode conversions that happen if a propagating Lamb mode interacts with several discontinuities. The selective actuation and receiving of wave modes, which make the interrogation process easier to quantitative identification of damage, provide only a partial solution to such problems. The complete suppression of other wave modes concerning the dominant mode is not guaranteed.

The conventional guided wave based SHM system commonly comprises of many sensors for accumulating the structural response. Raw signals, which contain the response of the structure, are obtained through sensors after transmission over a long distance. It is often corrupted by high frequency ambient random noise and coherent noise. These receieved signal, which often contains both types of noises, do not allow easy interpretation. All undesirable signal that exist in a repeatable mode whether or not there is a crack, fall in the category of coherent noise and these spurious signals misguide damage related analysis (Alleyne *et al*. (2000)). Besides the complexities inferred from the dispersion, multimode, and multi path characteristics of Lamb waves, interpretation of received signal becomes even more complicated when structures are subjected to various fluctuating operational (such as joint positions, rotating speed, flow rate) and environmental (humidity, temperature, wind) conditions (Clarke *et al.* (2008), Sohn (2007), Kullaa (2011), Dao and Staszewski (2013), Dao and Staszewski (2014), Liu *et al.* (2017)).Thus, signal processing and denoising techniques are essential to extract signal features from noisy signal before implementing in the damage identification algorithm to monitor the physical condition of the structures.

Over the years several signal processing and denoising techniques are developed to draw out useful information from contaminated signals.The filtering techniques, which are available in the open literature so far, are STFT (Ostachowicz *et al*. (2009), Wigner-

Ville distribution transform (Redouane *et al*. (2002), Dai *et al*. (2014)), and wavelet transform (Legendre *et al.* (2000), Sun and Chang (2002), Taha *et al*. (2006), Souza and Nobrega (2012), Zijian *et al*. (2016)). The most widely adopted one, which gained the attention of researchers in the last two decades, is the wavelet transform. It has been reported that (i) wavelet transform does not work well for SNR below 5 dB (Sun and Chang (2002)) (ii) coherent noise cannot be filtered by presently available averaging methods or wavelet denoising (Alleyne *et al*. (2000)) and (iii) signal processing with a optimal mother wavelet function can retain intrinsic features of the noisy measured signal (Li *et al*. (2009)).

To get over the limitations of the traditional wavelet transform based noise filtering technique (Srivastava et al. (2006), Adam (2010), Cohen (2012)), the authors initially developed the guided wave based matched filter for handling signal with low SNR and subsequently also developed the WMFM technique which couples both the wavelet transform and matched filter method. The novelty of the proposed method (WMFM) lies in the combination of the strength of wavelet and efficiency of matched filter in guided wave based SHM application. To the best of the knowledge of authors, so far no researcher has used this method. As the selection of an appropriate mother wavelet function is very crucial in the efficiency and accuracy of the signal transformation, the present analysis uses Shannon's entropy of wavelet coefficients and this selection is further justified by RMSE of filtered signal. Finite element method has been used to simulate wave propagation as well as reflection in the plate-like structure. The inspection of defect and the location of imperfection in the structure is worked out from the reflected signal. The Additive White Gaussian Noise (AWGN) is blended with the finite element simulated signal to get signal similar to experimental signal.

6.1.2 Mathematical formulation

6.1.2.1 Wavelet transform for denoising of signal

In case of NDT&E, wavelet transform used as a potent mathematical tool for analysing changes of structural integrity induced by discontinuities. The signal $x(t)$ is digitized as $x(n)$ which is split into two parts namely scaling coefficients and detail coefficients using multiresolution analysis. The wavelet representation of $x(n)$ comprises of a chain of all these approximations (Mallet (1998)). Multiresolution analysis $M = \{ V_j \subset L_2 \mid j \in J \subset Z \}$ consists of spaces V_j with Riesz bases given by the scaling functions $\{ \phi_{j,k} \mid k \in K(j) \}$ while a dual multiresolution analysis $\tilde{M} = \{ \tilde{V}_j \mid j \in J \}$ consists of spaces $\tilde{V}_j$ with Riesz bases given by dual scaling functions $\tilde{\phi}_{j,k}$. These dual scaling functions are biorthogonal with the scaling functions, in the sense that $\langle \phi_{j,k} , \tilde{\phi}_{j,k'} \rangle = \delta_{k,k'}$ *for* $k, k' \in K(j)$. The definition of multiresolution analysis implies that for every scaling function $\phi_{j,k}$ coefficients $h_{k,l}^{j}$ exist so that formally $\phi_{j,k} = \sum_{l \in K(j+1)} h_{k,l}^{j} \phi_{j+1,k}$. The dual scaling functions satisfy refinement relations with coefficients $\{ \tilde{h}_{k,l}^{j} \}$. Here a set of finite filters $\tilde{h}_{k,l}^{j}$ is considered. A set of functions $\{ \psi_{j,m} \mid j \in J, m \in M(j) \}$ is a set of wavelet functions if the spaces W_j = close span $\{ \psi_{j,m} \mid m \in M(j) \}$ is a complement of V_j in V_{j+1} and $W_j \perp \tilde{V}_j$. The dual basis is given by dual wavelets $\tilde{\psi}_{j,m}$ which are biorthogonal to the wavelets $\langle \psi_{j,m} , \tilde{\psi}_{j',m'} \rangle = \delta_{m,m'} \delta_{j,j'}$. The dual wavelets span spaces $\tilde{W}_j$ which complements $\tilde{V}_j$ in $\tilde{V}_{j+1}$ and $\tilde{W}_j \perp V_j$. Wavelets

satisfy refinement relations of the form $\psi_{j,m} = \sum_l g^j_{m,l}\, \phi_{j+1,l}$. Also, since $\phi_{j+1,k} \in V_j \oplus W_j$ it holds that $\phi_{j+1,k} = \sum_l \tilde{h}^j_{l,k}\, \phi_{j,l} + \sum_m \tilde{g}^j_{m,k}\, \psi_{j,m}$.

The biorthogonality condition gives the following relations between the filters:

$$\sum_l g^j_{m,l} \tilde{g}^j_{m',l} = \delta_{m,m'}, \sum_l h^j_{k,l}\, \tilde{g}^j_{m',l} = 0 \tag{6.1}$$

$$\sum_l h^j_{k,l}\, \tilde{h}^j_{k',l} = \delta_{k,k'}, \ \sum_l g^j_{m,l}\, \tilde{h}^j_{k',l} = 0 \tag{6.2}$$

Given scaling function coefficients C^{j+1}_k at level $j+1$, the wavelet coefficient d^j_k and scaling coefficient C^j_k at level j can be obtained as:

$$d^j_k = \sum \tilde{g}^j_{k,l} C^{j+1}_l;\ C^j_k = \sum \tilde{h}^j_{k,l} C^{j+1}_l \tag{6.3}$$

Now the inverse transform can be applied by

$$C^{j+1}_k = \sum_m h^j_{m,k} C^j_m + \sum_l g^j_{l,k} d^j_l \tag{6.4}$$

Figure 6.1 shows the layout of the two levels of resolution filter bank for DWT. A High Pass (HP) filter decomposes the signal into details while a Low Pass (LP) filter decomposes the signal into approximations. The signal reconstruction process is shown in another half of the figure, which synthesizes the DWT coefficients assembled back to the original signal without loss of information by using Reverse Low Pass (RLP) and Reverse High Pass (RHP) filter. This signal reconstruction process can be performed by the Inverse Discrete Wavelet Transform (IDWT).

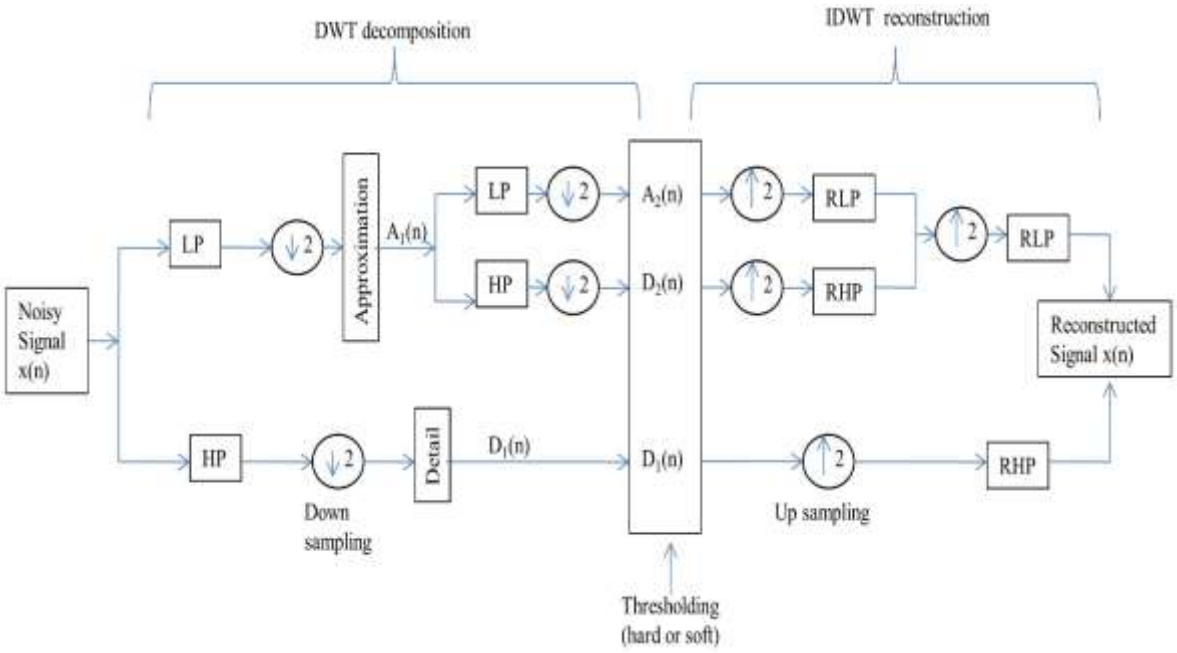

Figure 6.1 Two level filter bank for DWT analysis

The wavelet transform of the Lamb wave signals is investigated in the present work by using a fast orthogonal and biorthogonal wavelet transform algorithm reported in Donoho, (1995) and with the help of a library of MATLAB routines for wavelets. In order to denoise the signal, thresholding of the wavelet coefficients is employed on the detail coefficients. This noise removal method was initially introduced by Donoho and Johnstone (1994). The rules for hard and soft thresholding are given as

Hard thresholding:
$$\left(d^{j}\right)=\begin{cases} d^{j}, & if \quad \left|d^{j}\right|>\lambda \\ 0, & if \quad \left|d^{j}\right|\le\lambda \end{cases} \tag{6.5}$$

Soft thresholding:
$$\left(d^{j}\right)=\begin{cases} d^{j}-\lambda, & if \quad d^{j}>\lambda \\ 0, & if \quad \left|d^{j}\right|\le\lambda \\ d^{j}+\lambda, & if \quad d^{j}<-\lambda \end{cases} \tag{6.6}$$

where λ represents thresholding of wavelet coefficient.

It is well established that in order to obtain better output signal, the selection of the thresholding method as well as threshold values is a critical issue. Even though hard and soft thresholding rules make the coefficients zero when absolute values are lower than the threshold, however the soft thresholding rule, additionally, shrinks the coefficients above the threshold. Again, as the selection of large threshold value cuts too many coefficients, thereby leading to an over smoothing and on the other hand too small threshold value permits annoying blips in the curve, Donoho and Johnston (1994) formulated a variety of threshold preferring methods. As the present analysis focuses on white Gaussian random noise, in order to remove the noise we can effectively use universal thresholding rule from the above reference as $\lambda^{Universal} = \hat{\sigma}\sqrt{2\log \mathrm{n}}$, where n is the length of the coefficients, and $\hat{\sigma}$ is an estimate of the standard deviation of the noise level σ . The estimate $\hat{\sigma}$ is dependent on the last level of the detail wavelet coefficients since it contains noise. Donoho and Johnston, 1994 suggested an adequate estimate $\hat{\sigma}$ of the noise level σ as

$$\hat{\sigma} = \frac{MAD(\left|d_{j-1}, k\right| : k = 0,1,...,2^{j-1}-1)}{0.6745} \tag{6.7}$$

Where the scale factor 0.6745 is for a normal distributed data and *MAD* is median absolute deviation. The scale factor is counted on the distribution of detail wavelet coefficients. Depending upon the variation in noise level σ the estimator will be keep on changing.

6.1.2.2 Matched filter and wavelet matched filter methods

In this section, at first we introduce the concept of the MFT and later on develop a new approach called WMFM where initially denoised signals from wavelet transform are further processed through the route of matched filtering to enhance the quality of the final output signal. In MFT, the important part of any signal containing noise is obtained

by convolving the unknown signal with a conjugated time-reversed version of the known signal, or template. In the presence of stochastic noise, the matched filter maximizes the output SNR. The idea behind the matched filter relies on choosing a filter that is orthogonal to the noise. In other words, the inner product of received signal with a known expected signal will be maximum if received signal is parallel with the expected signal (Minkoff 2002).

In this study finite element method has been used to generate the signal on a structure containing a defect. The simulated signal *s*(t) is overlapped with white Gaussian noise $\eta(t)$ with two-sided constant power spectral density $N_0/2$.Now, the output signal *y*(t) of matched filter is calculated by convolution of the noisy signal as demonstrated below.

$$\mathrm{y}(t) \;=\; \left[s(t)+\eta(t)\right]*h(t) \;=\; y_s(t)+y_\eta(t) \qquad (6.8)$$

Here, $y_s(t)=\int_0^t s(\tau)h\left(t-\tau\right)d\tau$ represents the useful information of the signal and $y_\eta(t)=\int_0^t \eta(\tau)h\left(t-\tau\right)d\tau$ the noise component. The impulse response *h(t)* of the matched filter is the inverted form of the simulated signal *s*(t), given as $h(t)=\pm cs(t-\tau)$. Consequently, the SNR in this case is then given as

$$SNR=\frac{y_s^2\left(t\right)}{\in\left[y_\eta^2\left(t\right)\right]}=\frac{\left[\int_0^t s(\tau)h\left(t-\tau\right)d\tau\right]^2}{\frac{N_0}{2}\int_{-\infty}^{\infty}h^2\left(t-\tau\right)d\tau} \qquad (6.9)$$

where $\in$ is the statistical expectation.

The basic functioning of the WMFM is based on the details explained in section 6.1.2.1 and beginning of the current subsection. In this method, a unique combination of wavelet thresholding algorithm and convolution approach is developed for the detection of damage explicitly taking into account noise due to multiple reflections and varying environmental and operational conditions. In this approach the contaminated signal is first decomposed into wavelet coefficient and scaling coefficient using DWT filter bank using Equation (6.3). Thereafter, we performed thresholding for wavelet coefficient using Equation (6.5) and Equation (6.6) and subsequently signal is reconstructed using Equation (6.4). Now we move to use the matched filter which convolutes the reconstructed signal available from wavelet transform with healthy signal through Equation (6.8) in order to generate the final enhanced output signal $y_s(t)$. Figure 6.2 outlines the block diagram of the newly proposed WMFM.

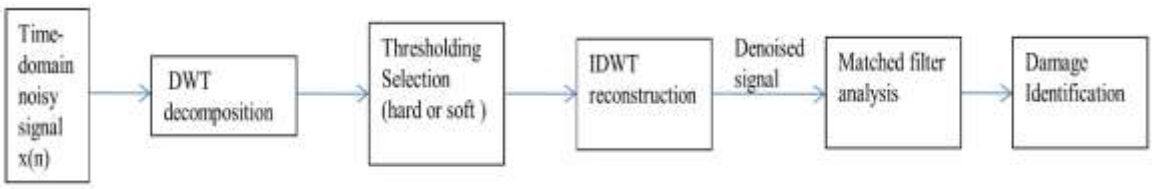

Figure 6.2. Proposed WMFM for damage identification

6.1.2.3 Criteria for selecting the optimal wavelet using Shannon's entropy

Shannon's entropy evaluates the randomness or energy dispersion in a closed system. In other worlds, it shows the energy concentration or degree of uncertainty (Shannon, 1994). This criterion can be applied as an indicator of appropriate wavelet function among all available orthogonal and biorthogonal wavelet for analyzing Lamb wave signals (Li *et al*., 2009). Shannon's entropy not only provides optimal mother

function but also depicts the transform level of detail. The Shannon's entropy of detail at transform level *l* can be defined as

$$S_{(j)} = \sum_{i=1}^{n} \left(\frac{\left(d_i^j\right)^2}{D} \ln \left(\frac{\left(d_i^j\right)^2}{D} \right) \right) \tag{6.10}$$

Where, $D = \sum_{j=1}^{L} \sum_{i=1}^{n} \left(d_i^j\right)^2$. Here, L is the maximum transform levels of wavelet used in the analysis. The obtained wavelet coefficients at a transform level j are given by d_i^j and n is the length of the input signal. The optimal wavelet function should always yield minimum value of the Shannon entropy for the noisy signal.

6.1.3. Results and discussion

In this section, we examine the guided Lamb wave propagations in structures without and with damage. In order to evaluate the performance evaluation of the filtering techniques, it is decided to examine contaminated signal with SNR of 20, 15, 10, 5, 0, -5, -10, -15 and -20 dB. In this experiment, AWGN is added to the FE simulated signal for the plate to get signal similar to the experimental signal, and resulting signals are analyzed using various filtering techniques. We present the enhancement on crack detection process by implementing matched filtering technique, wavelet matched filter method, and wavelet based DWT and CWT as data post-processing tools. Several wavelet function and thresholding methods are also tested on contaminated signals, as well as Shannon's entropy criterion is selected to calibrate degree of optimal wavelet function and justified by RMSE for denoising the signal. Estimated value of correlation coefficient and RMSE

is tabulated to establish effectiveness and acceptability of proposed method. The potential of the proposed method is analyzed using several examples.

6.1.3.1 Single wave mode excitation

(a) Finite element simulation

Three-dimensional finite element model of Al plate (1000 mm length, 40 mm wide and 2 mm thickness) is considered. Commercial FEM code ABAQUS (an explicit time integration FE solver) is used to numerically simulate the propagating and scattering phenomena of Lamb wave propagation as shown in Figure 6.3. The position of a sensing point and crack are demonstrated in the same figure. The number of simultaneously existing modes increases as the center frequency of excitation increases. The center frequency of excitation is generally maintained relatively low to restrict the number of coexisting modes. In the present study, to compute the response of wave interaction under excitation frequency 100 kHz, the FE model is excited by imposing a time-varying pin force in the 'in-phase' along x-direction on all intermediate nodes (through the thickness) of the left edge. The actuation function is driven through a Hanning- window (Greve *et al.* (2005)) as

$$F(t) = \begin{cases} f_o \sin(\omega t) * \left(\sin(\frac{\omega t}{10}) \right)^2, & t < \frac{10\pi}{\omega} \\ 0, & otherwise \end{cases} \qquad (6.11)$$

Where f_0 is the maximum amplitude, ω is the center frequency of excitation. The following material properties of Al are assumed to generate dispersion curves: Poisson's ratio=0.33; density=2700 kg/m^3; Young's modulus E=69 GPa. The phase velocity, approximately 5050 m/s, is obtained for S_o wave from the dispersion curve, so the

wavelength at 100 kHz will be about 50.5 mm. The element length of 1 mm and discrete time increment $1\times10^{-7}\,s$ is adopted for numerical stability and computational efficiency. The healthy plate and cracked plate are discretized using eight node linear brick elements type C3D8R with first-order reduced integration.

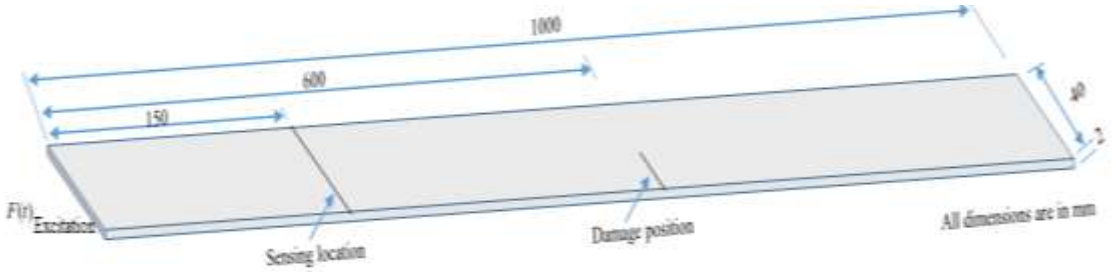

(a) Plate geometry

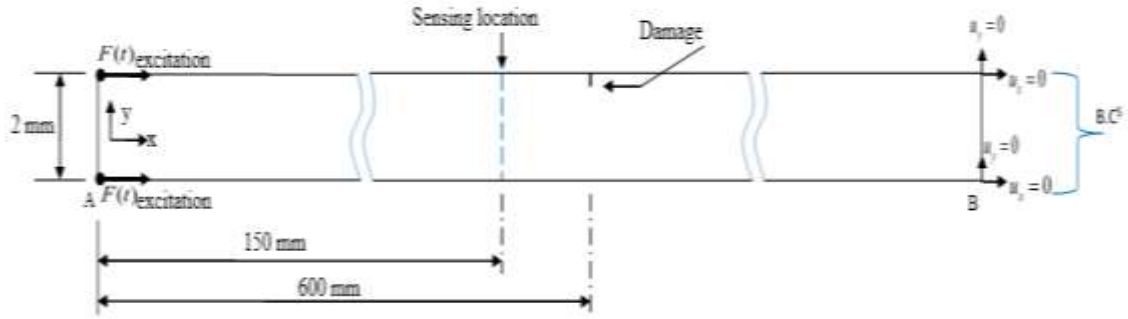

(b) FE model, boundary conditions, forcing function and damage

Figure 6.3. Schematic of FE model

In spite of many favorable characteristics of guided-waves, the dispersion is inevitable. Therefore, windowed 5 cycle sinusoidal tonebursts with relatively narrow bands are employed as incident signals in guided wave applications to decrease the effect of dispersion (Li et al. (2006)). The first simulation is performed for a healthy plate; next simulation is carried out to investigate effects of flaw on the damaged plate with 1mm wide and 1mm deep square notch. The monitoring time is selected to record the small number of reflections coming from the edges of the structure. Therefore, the damage

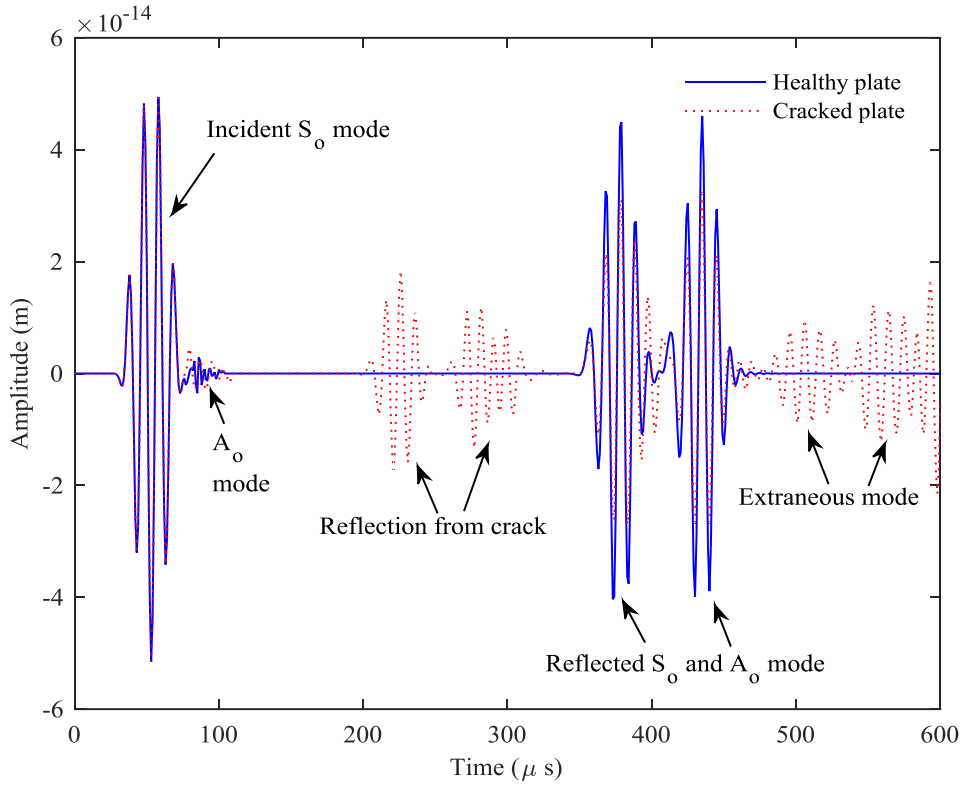

Figure 6.4. Sensor output for S_0 mode excitation for the healthy and damage plate

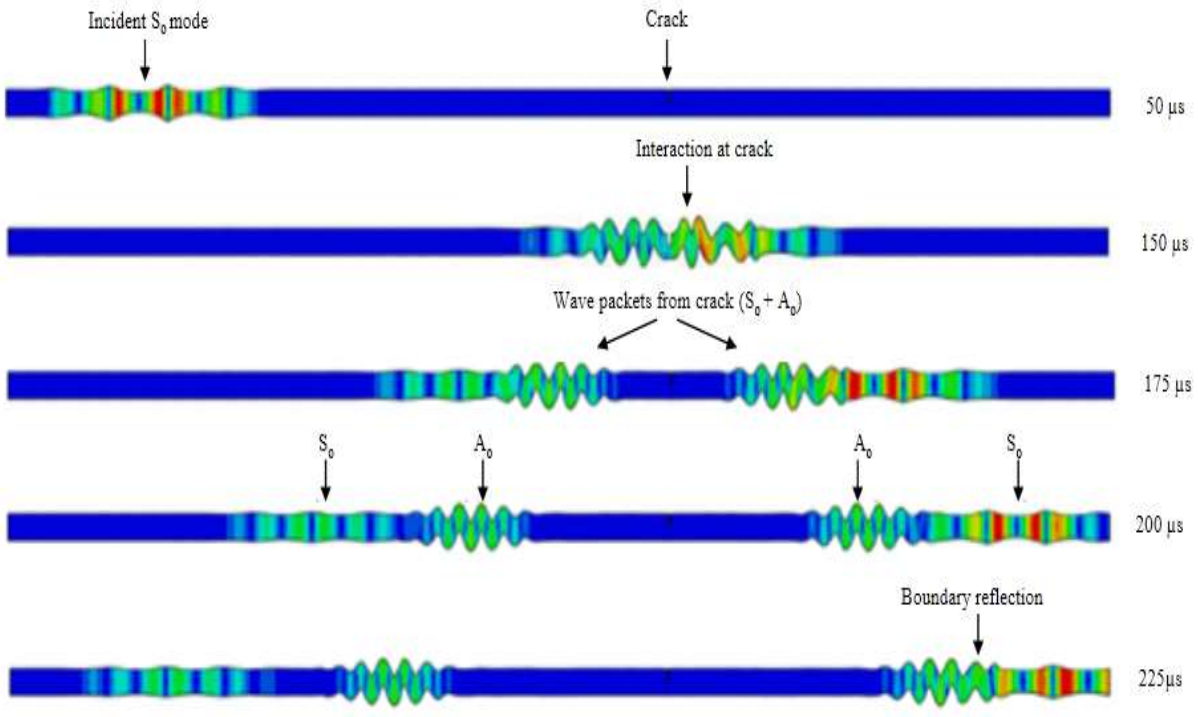

Figure 6.5. FE simulation of Lamb wave

detection of the plate becomes easier because of the presence of a limited reflection. The measured response of time-domain signals from FE simulation for a healthy plate and damage plate is shown in Figure 6.4. It can be distinctly examined that new wave modes appeared in the time-domain signal received from the damaged plate. Damage is observed by analyzing echoes in the received response due to wave reflections away from damaged regions. Typical snapshots of Lamb wave propagation in the damaged plate with different times frame are demonstrated in Figure 6.5.

(b) Optimal selection of mother wavelet function

To find a suitable wavelet filtering technique, various orthogonal and biorthogonal wavelets with multiple thresholding are tested for filtering of the signal. DWT and CWT contain the broad spectrum of wavelets and scaling functions; biorthogonal (bior4.4), Coiflet (coif5), Daubechies (db4), Discrete Meyer (dmeyr) and Symlet (sym5) wavelets are utilized in this data processing. In order to decide the optimal wavelet, initially we plot the Shannon's entropy and subsequently the RMSE is compared for various wavelet functions. Figures.(6.6, 6.7) represent calculated Shannon entropy with respect to transform level for different wavelet functions (using Eq.6.10) based on DWT and CWT in both the healthy and damage plate signals.

Shannon's entropy curves of the simulated signal using different DWT wavelets are compared in Figures 6.6(a, b). Two troughs are present in the curves, located at the scales 1 and 5. The low value of entropy received for the first level of scale, because of the noise contained higher frequency components than the signal. Although the chosen wavelets yielded almost identical entropy with constant value at higher transform level, there are significant differences in the results obtained from various wavelets at lower

scale. It is observed that db4 represents the lowest trough in case of DWT, Figures 6.6(a, b) while, on the other hand Morlet wavelet produces the lowest trough for the CWT based wavelet functions as shown in Figures 6.7(a, b) for both the healthy and damaged plate signals. The lowest value of Shannon entropy delivers one of the best wavelet functions (db4 in DWT and Morlet in CWT) to be used for the processing of the signal. It can also be noticed that Shannon entropy curves of the healthy plate and cracked plate produce identical curves for DWT and CWT based wavelet functions. It indicates that the optimal wavelet function and the transform level is the same, for same incident Lamb wave signal and it is possible to choose the best wavelet from the healthy plate signal if the incident wave is same for denoising of any damaged plate signals.

To further examine the reliability of the chosen wavelet functions based on Shannon's entropy criterion, we plot RMSE with respect to various SNR values, Figures. 6.8(a-c). The RMSE is defined as $RMSE = \sqrt{\frac{1}{n}\sum_{i=1}^{n}\left(O_{(i)} - d_{(i)}\right)^2}$; where, $O_{(i)}$ is the noise free signal, $d_{(i)}$ is the denoised signal and *n* is the number of the signal point. The RMSE values are diminishing with increase in SNR as expected in all the cases. It is reflected in Figures 6.8(a) and 6.8(b) based on soft and hard thresholding, respectively that db4 produces the minimum error among the selected wavelet functions for the current range of SNR values. In case of CWT based wavelet functions, as shown in Figure 6.8(c) the minimum error is observed in Morlet wavelet. It is also notable that the performance of Haar wavelet is not suitable for both DWT and CWT based processing of Lamb wave signals.

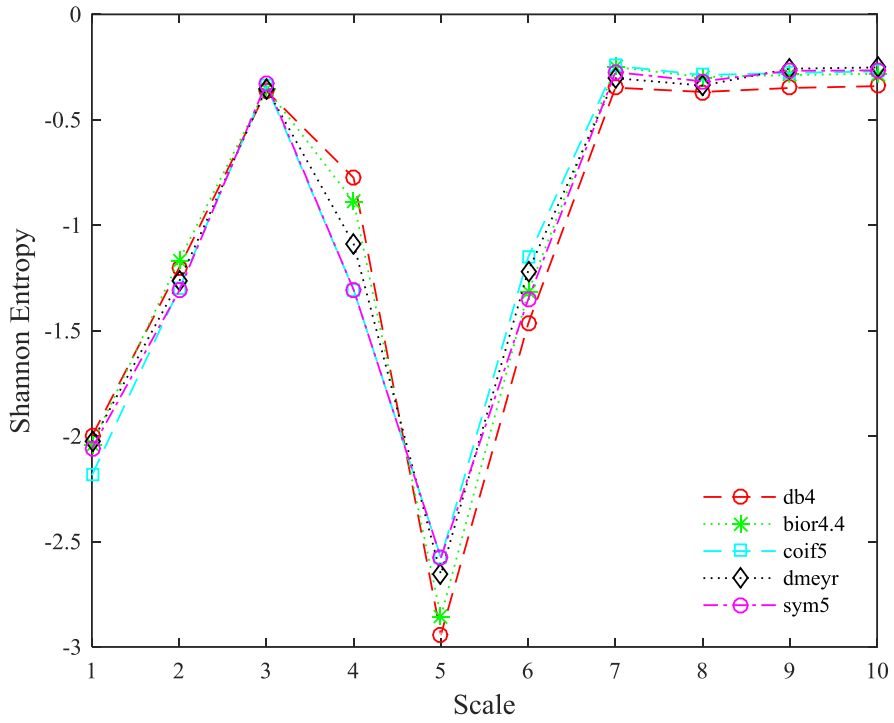

(a) healthy plate

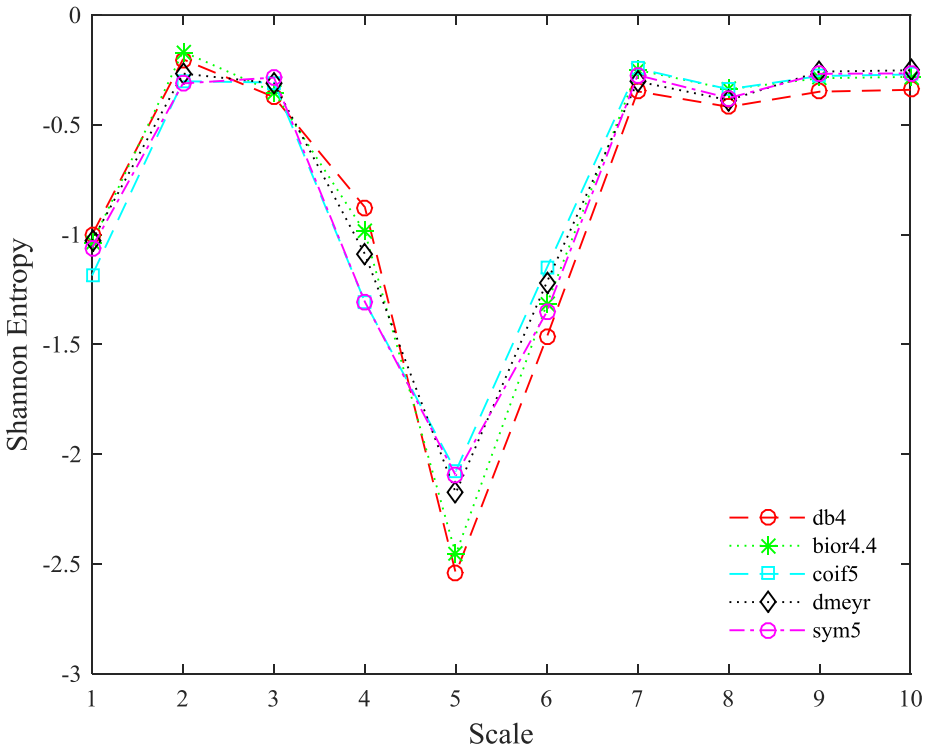

(b) damaged plate

Figure 6.6. Shannon's entropy curves of the DWT from Lamb wave signal

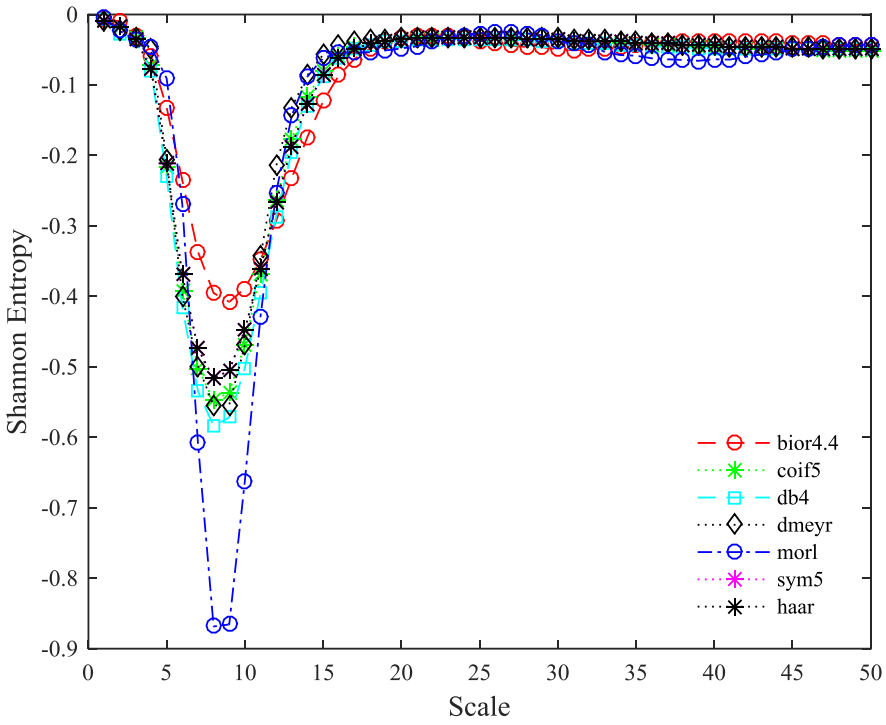

(a) healthy plate

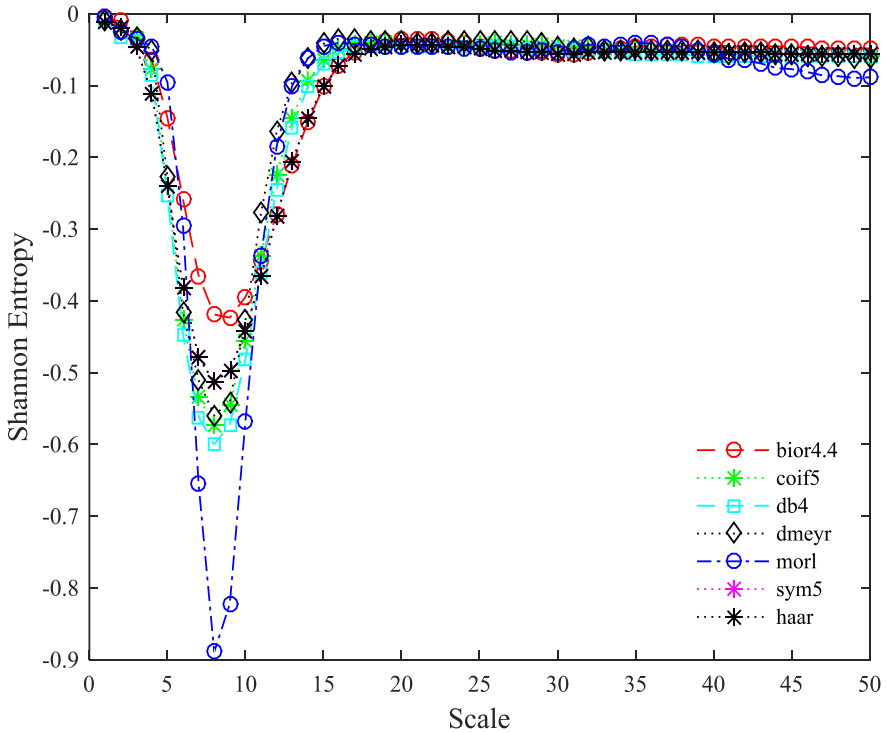

(b) damaged plate.

Figure 6.7. Shannon's entropy curves of the CWT from Lamb wave signal

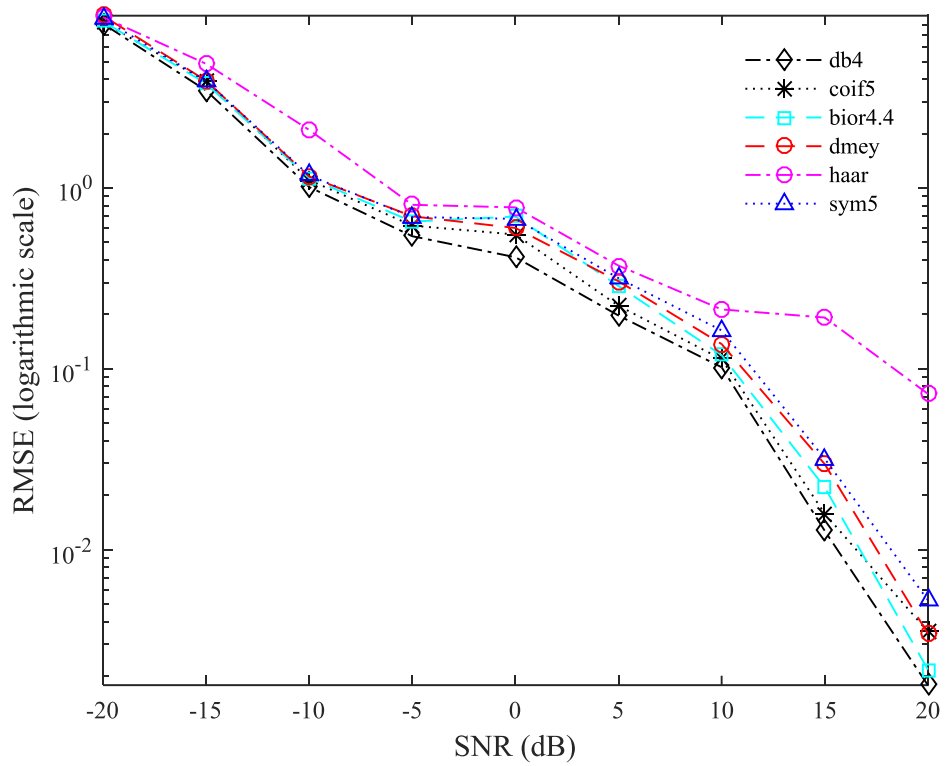

(a) DWT with soft thresholding

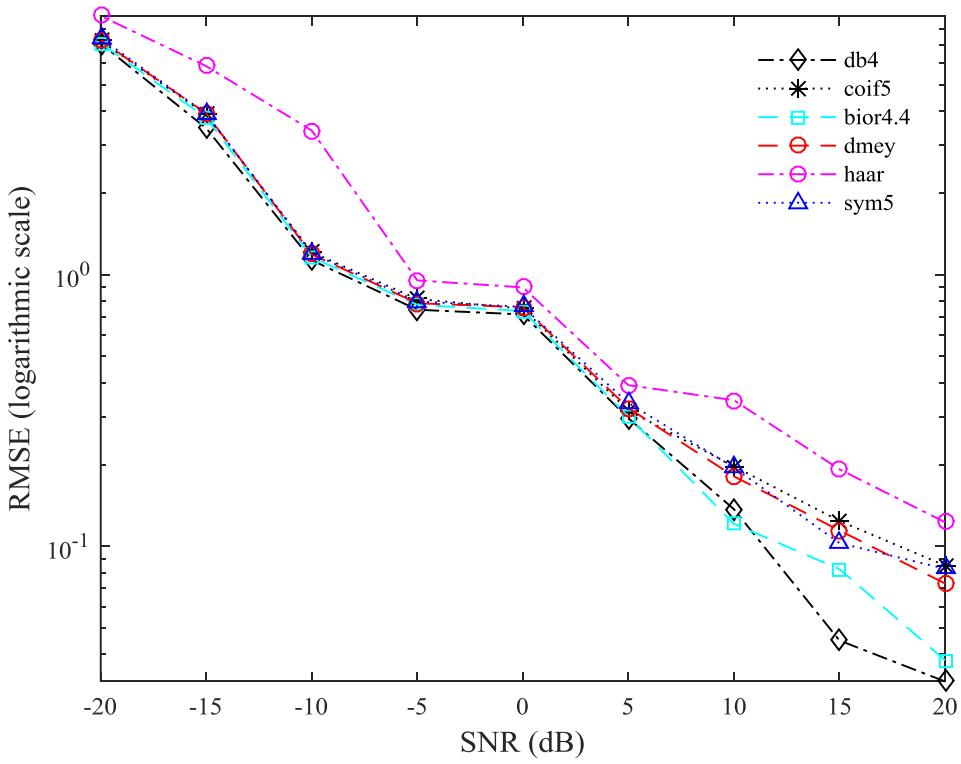

(b) DWT with hard thresholding

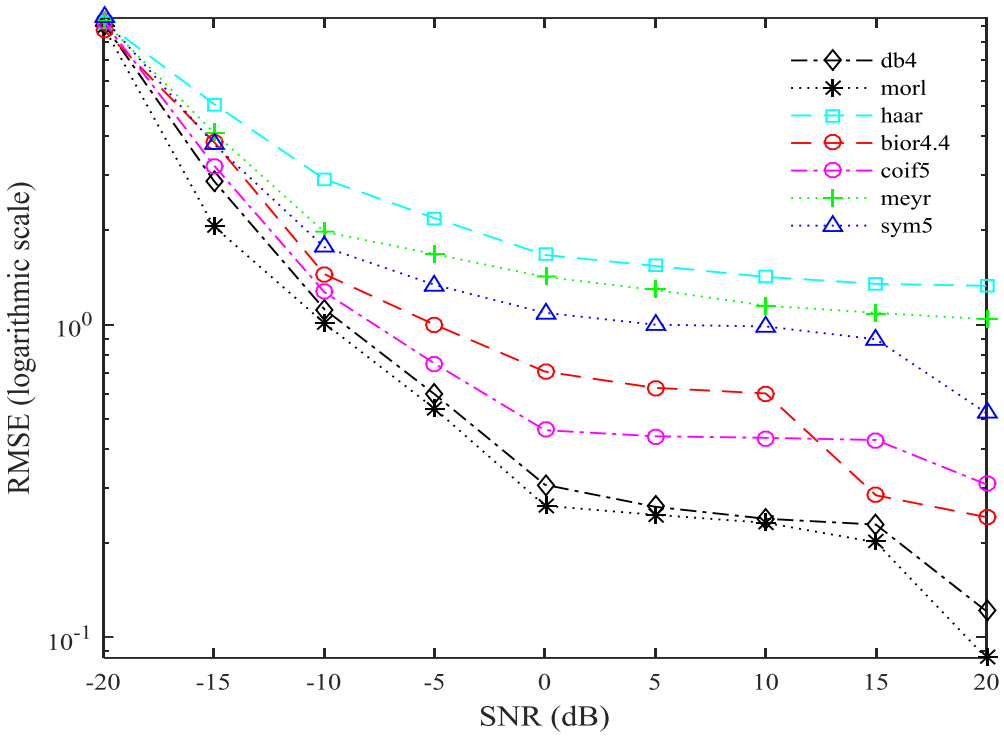

(c) CWT

Figure 6.8. RMSE in various SNR level computed from wavelet transform

(c) Denoising and damage detection results using three different filtering techniques

Based on the optimal choice of wavelet function, now we present the performance of the wavelet transform and MFT together with the performance rendered by WMFM for the damage structure signal. Figure 6.9 shows the contaminated signal of damage structure for the case of SNR of 0 dB and it can be observed that the original signal is lost in the noise whereas Figures (6.10-6.12) present denoising of this contaminated signal via the three filtering techniques based on wavelet transform, MFT and WMFM, respectively.

In Figure 6.10, denoising is performed using Morlet and DWT based db4 wavelets. This figure reflects that the wavelet transforms are unable to detect properly the signal due to damage in the structure through DWT based wavelet. A shortcoming of wavelet transform in context of analysis of transient responses is the compromise in the

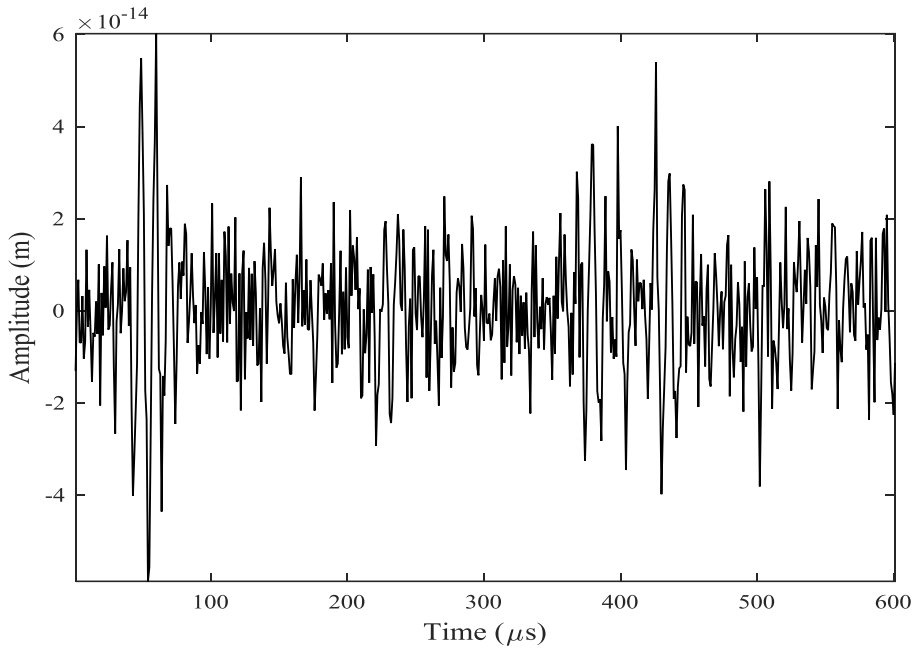

Figure 6.9. A contaminated signal with SNR 0 dB for damage plate

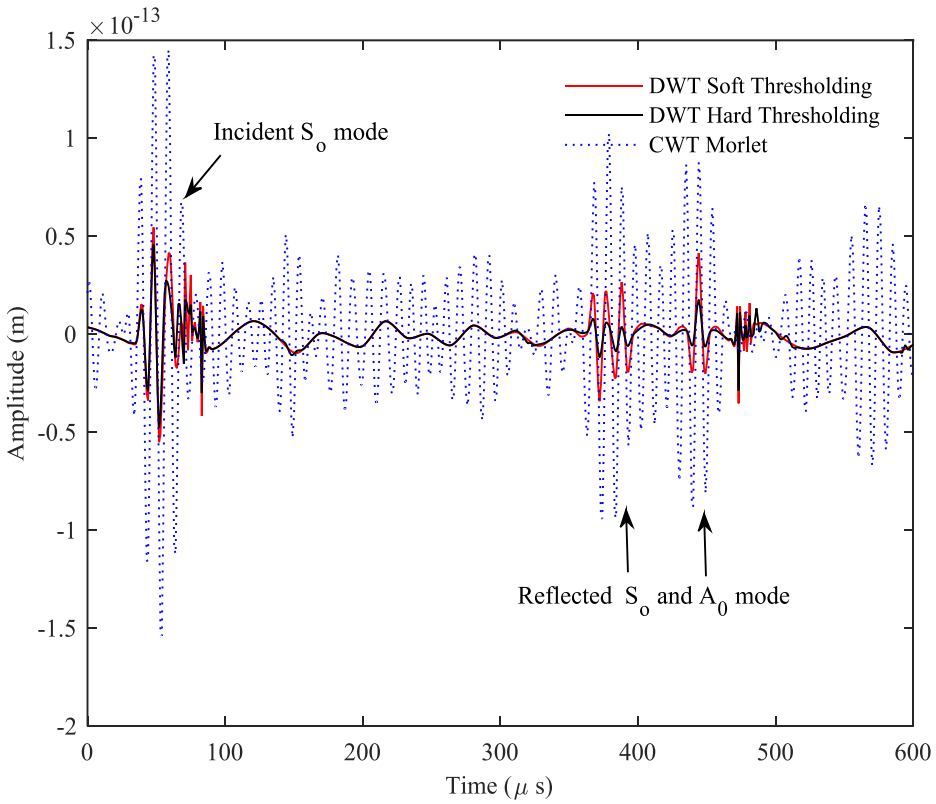

Figure 6.10. Wavelet transform for the contaminated signal with SNR (0 dB) for damaged plate

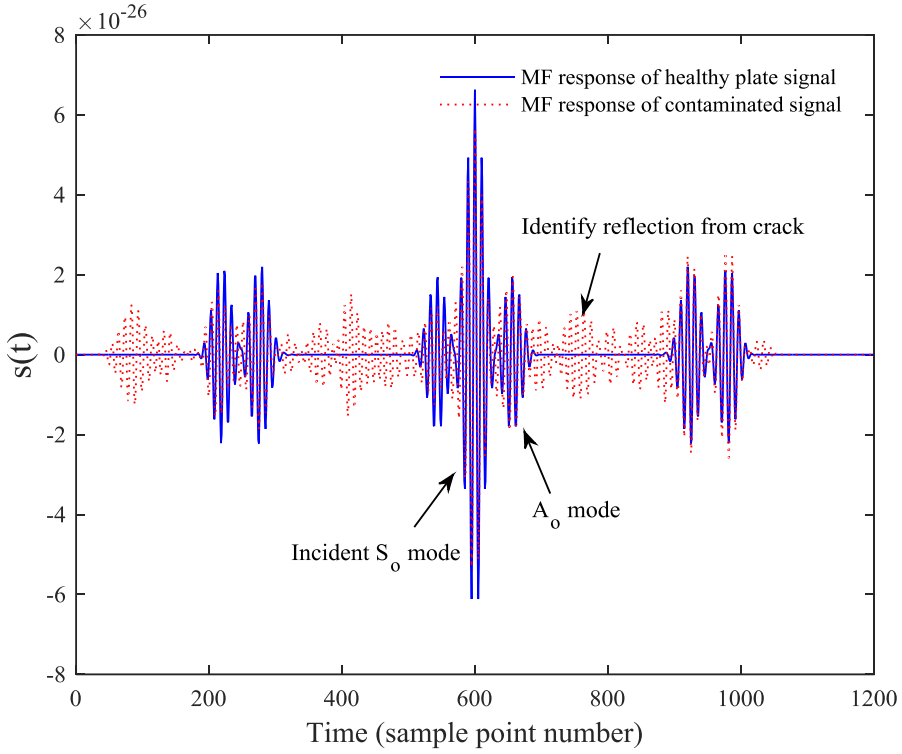

Figure 6.11. Contaminated signal with SNR (0 dB) convoluted with healthy plate signal

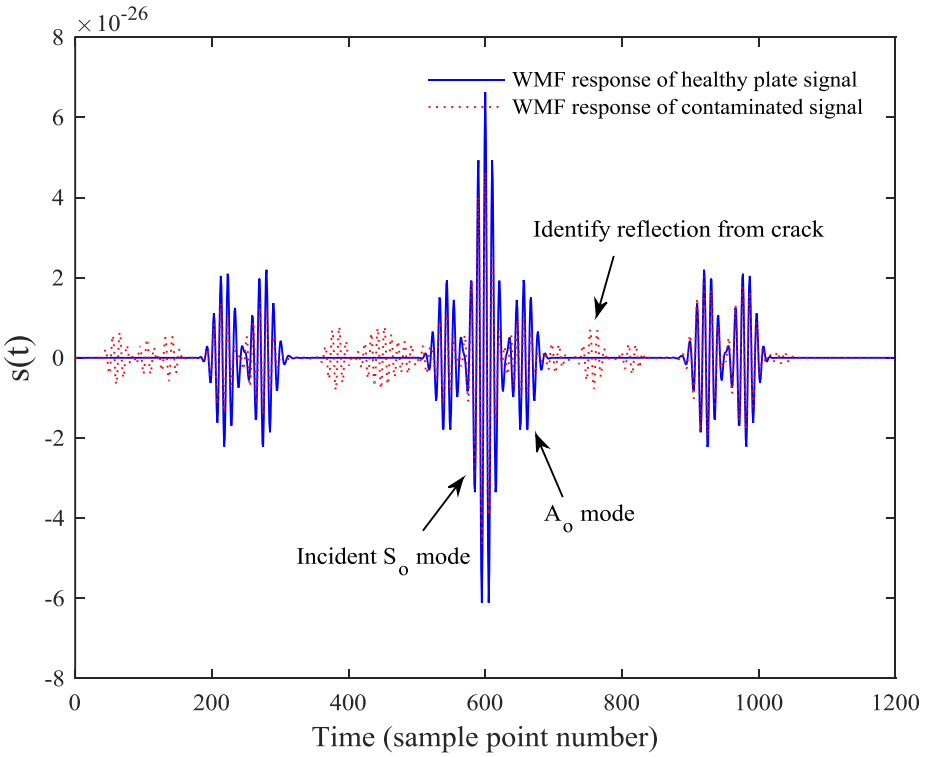

Figure 6.12. The response of wavelet matched filtering for the signal with SNR (0 dB)

frequency resolution for enhanced time resolution and vice-versa (Pai et al., 2015). However, when the same noisy signal is processed by the MFT the filtered response demonstrates improvement in denoising as compared to the wavelet transform method. Here, In Figure 6.11, convolution of the healthy plate signal without noise (blue color), as obtained from FE simulation, considered as $y_s(t)$ of Eq. 6.8 is compared with $y(t)$ of contaminated signal (red color). Matching of the red color signal with the blue color signal indicates the presence of the desired response from the noisy signal; in this case the reflection from the damage is clearly visible. This result shows how convolution could improve the resolution of the time domain signal. Therefore, the damage detection of the structure becomes easier. However, some unwanted wave packets are visible in the final output signal. In Figure 6.12, we plot the output response obtained through the use of WMFM. This Figure shows WMFM work very efficiently under the uncorrelated noisy signal because in this technique the advantages of both the methods mentioned above were used in the computation and finally an improved response is achieved. The method not only helps to detect easily the signal due to the presence of defect but also shows that unnecessary extra wave packets are suppressed to a large extent. It can be concluded from this study that even though most of the earlier and current studies related to SHM use wavelet transforms to process the noisy signal, but the use of MFT and the newly developed concept of WMFM can be more confidently used for identification of damage than the previous methods.

The performance of these filtering technique is also evaluated in the presence of coherent noise and shown in Figures (6.13-6.16). The monitoring time is increased in FEM simulation to trace the multiple reflections coming from the edges and discontinuities of the plate. Figure 6.13 shows the time domain signal which is

complicated by the presence of strongly overlapping reflections along with random noise. Though this time trace is measured on a simple thin plate, it is very difficult to analyze and can be considered as representative of the typical real-world signals of the complex structures. Similar structural response signals are presented by Han et al. (2009), Sorohan et al. (2007), Lu et al. (2006). Denoising of this polluted signal (Figure 6.13) by using wavelet based filtering is shown in Figure 6.14. Wavelet based filtering method is only able to filter the random noise but unable to remove extraneous mode which represents the coherent noise. On the other hand, MFT and WMFM are not only able to remove random noise but also filtering the coherent noise as demonstrated in Figure 6.15 and 6.16. Comparing the responses as received by the present filtering methods, here, again we can notice that WMFM help to suppress the noise part to much greater extent and facilitate to detect the flaw easily. In this case it is further observed that the wavelet transform is able to filter only the random noise, whereas the other two techniques are not only suppressing the random noise but also preventing the coherent noise, simultaneously.

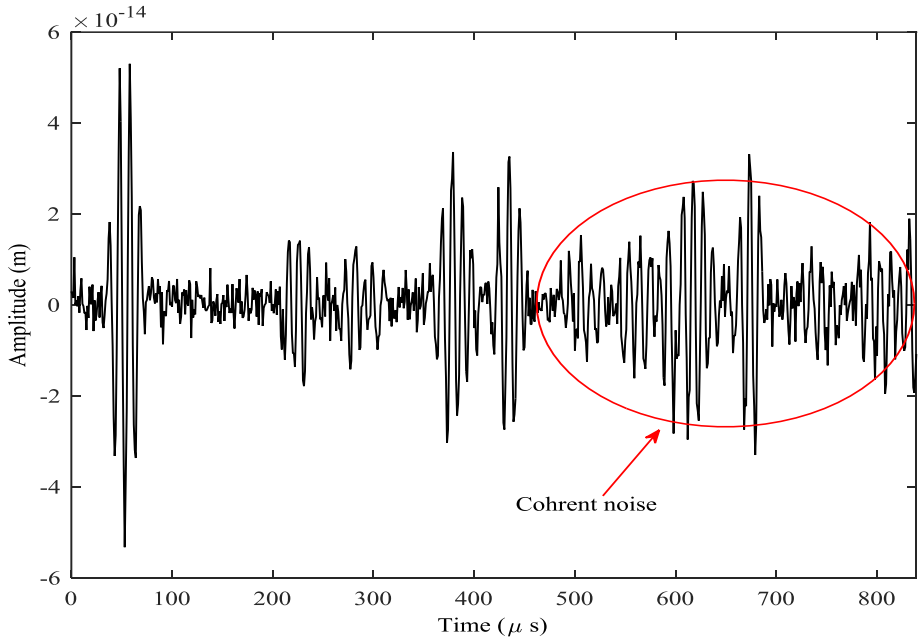

Figure 6.13. A contaminated signal with SNR (10 dB) and coherent noise

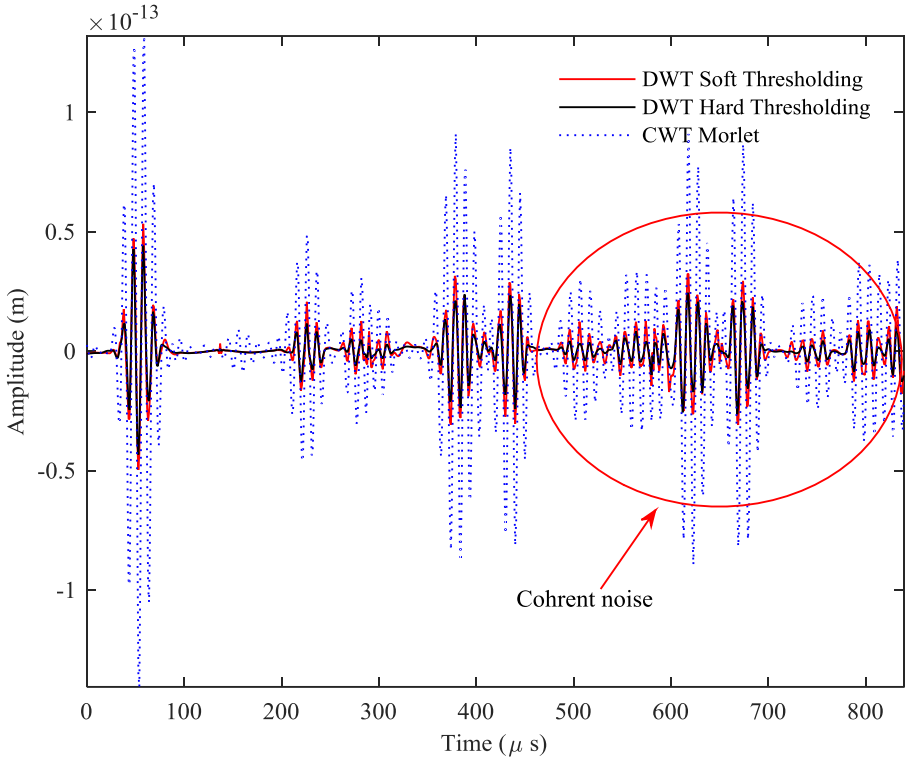

Figure 6.14. Wavelet transform for the contaminated signal with SNR (10 dB) and coherent noise

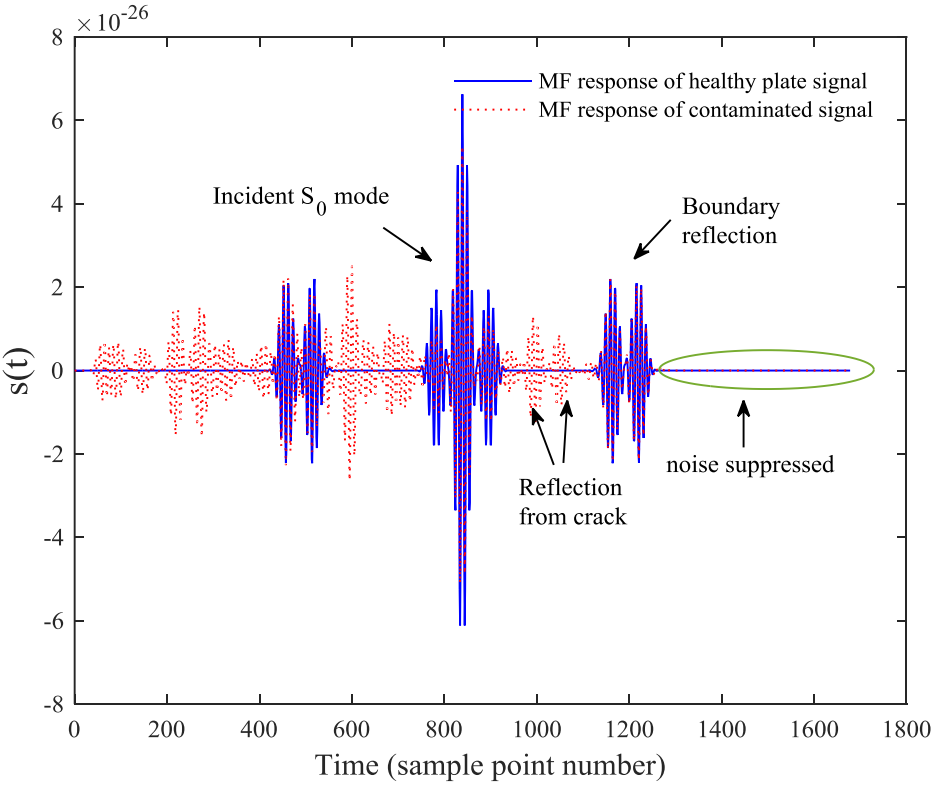

Figure 6.15. MFT response for the contaminated signal with SNR (10 dB) and coherent noise

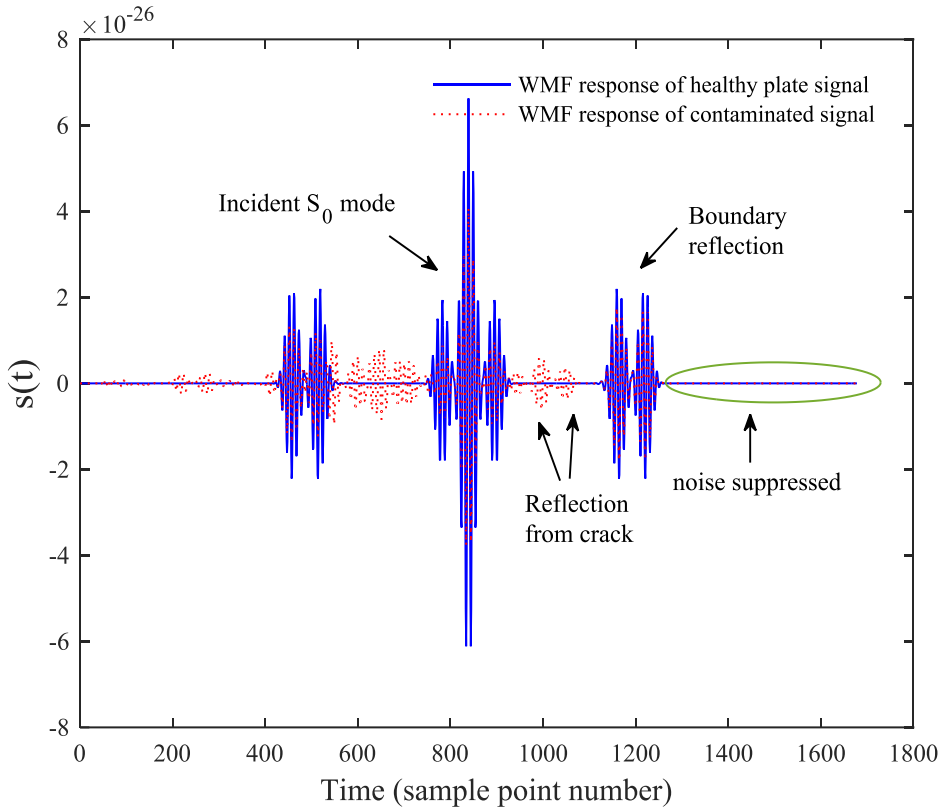

Figure 6.16. WMFM response for the contaminated signal with SNR (10 dB) and coherent noise

(d) Validation using statistical tools

To compare the efficiency of the proposed filtering techniques and to comment upon whether the output signals are within the acceptable limit or not (using correlation coefficient and RMSE, we demonstrate the correlation coefficient of the processed signal with respect to noise free signal in Tables (6.1-6.3) for all the three methods. The RMSE and enhanced values of the SNR are also computed to take closer look and put in the tables to reflect the effectiveness. The linear correlation coefficient is a statistical method that can measure the relation between two variables. Here, the correlation coefficient predicts how well denoised signal follows the noise free signal. Correlation coefficients can vary from -1.00 to +1.00. The correlation coefficient is defined (Dallal (2012), Fisher (1954)) as

$r = \sum_{j=1}^{N}(x_j - \bar{x})(y_j - \bar{y}) \Big/ \sqrt{\sum_{j=1}^{N}(x_j - \bar{x})^2 \sum_{j=1}^{N}(y_j - \bar{y})^2}$; here x_j and y_j are original signal and denoised signal, respectively; $\bar{x}$ and $\bar{y}$ represent mean of original signal and denoised signal, respectively.

Table 6.1 presents the calculated correlation coefficients and RMSE values for the wavelet-based hard and soft thresholding methods with various SNR from 20 dB to -20 dB. It can be observed that denoising results are acceptable according to estimated value of the correlation coefficient. Also, denoising method is productive if Post SNR is higher than Pre SNR. Table 6.2 is constructed for matched filtering technique in order to evaluate denoising ability with various SNR and it is evident that the proposed matched filtering method is performing better than the wavelet based denoising with notable correlation coefficient values. Table 6.3 gives a complete comparison of the wavelet matched filter method with the hard and soft thresholding.

Table 6.1. Comparison of RMSE, correlation coefficient and post improved SNR of the wavelet denoising

SNR(dB) (before filtering)	Hard thresholding			Soft thresholding		
	RMSE	Correlation coefficient (*r*)	SNR (dB) (after filtering)	RMSE	Correlation coefficient (*r*)	SNR(dB) (after filtering)
20	0.0257	0.9888	31.89	0.0186	0.9897	32.19
15	0.049	0.9815	26.19	0.0435	0.9868	30.52
10	0.129	0.9732	22.52	0.0967	0.9817	24.75
5	0.346	0.9673	15.79	0.237	0.9792	18.59
0	0.751	0.9535	7.66	0.549	0.9157	11.28
-5	0.745	0.7746	3.38	0.627	0.8065	3.24
-10	1.34	0.6465	-2.625	0.915	0.7127	0.13
-15	3.92	0.1878	-8.34	3.68	0.3543	-8.25
-20	7.79	0.1237	-14.83	7.56	0.1079	-12.94

Table 6.2. Comparison of RMSE, correlation coefficient and post improved SNR of the MFT

SNR(dB) (before filtering)	Matched filtering technique		
	RMSE	Correlation coefficient (*r*)	SNR (dB) (after filtering)
20	0.00553	0.9898	34.32
15	0.0231	0.9877	30.89
10	0.0563	0.9787	24.98
5	0.195	0.9762	19.01
0	0.352	0.9622	11.82
-5	0.613	0.8485	5.12
-10	0.957	0.7236	0.031
-15	4.114	0.4513	-3.22
-20	7.611	0.2306	-9.16

Table 6.3. Comparison of RMSE, correlation coefficient and post improved SNR of the WMFM

SNR(dB) (before filtering)	Wavelet matched filter method					
	Hard thresholding			Soft thresholding		
	RMSE	Correlation coefficient (*r*)	SNR(dB) (after filtering)	RMSE	Correlation coefficient (*r*)	SNR(dB) (after filtering)
20	0.00625	0.988	36.25	0.00649	0.9898	37.38
15	0.0219	0.9827	31.61	0.0159	0.987	33.81
10	0.0578	0.9773	24.83	0.0438	0.9862	25.15
5	0.139	0.9759	17.47	0.125	0.9769	20.52
0	0.387	0.9648	11.33	0.347	0.9718	12.73
-5	0.496	0.8537	7.48	0.523	0.8688	8.17
-10	0.832	0.7515	0.37	0.781	0.7656	1.73
-15	2.357	0.4853	-3.27	1.87	0.4827	-2.25
-20	4.181	0.2968	-8.51	4.262	0.3145	-8.21

In all SNR cases, the WMFM indicates superior performance compared to the existing methods. From the tables we can conclude that the correlation coefficients are within the limit for all the three methods; however, the coefficient values deteriorate to a large extent below SNR of 0 dB. In case of other two parameters while comparing the

RMSE and SNR values of denoised signal, similar trends are visible. Finally, from all the three tables, while comparing the correlation coefficient, RMSE and SNR values of filtered signal, we can bring into notice of readers that the new concept of WMFM technique may be a very suitable filtering method in dealing the signals under consideration and to obtain a reliable noise free signal.

6.1.3.2 Multi wave mode excitation

(a) Finite Element Simulation

Plane strain finite element model of Al plate ($l \times h$=800×2 mm) is considered in the present analysis and simulated using the commercial FEM software ANSYS for the Lamb wave propagation as shown in Figure 6.17. The position of a sensing point and damage are demonstrated in the figure. To provide a limited cycle sinusoidal tone burst, $5\frac{1}{2}$ cycle Hanning-window sine burst excitation signal is applied for modes propagation. The healthy plate is discretized using 2D four node plane strain bilinear quadrilateral element of type PLANE 182 with reduced integration and plate with defect of notch is also discretized using similar elements. As a compromise between solution accuracy and computation time a grid of elements 11483 with 13527 nodes are chosen and the element length selected near the damage was of 0.2 mm. In the simulation a discrete time increment of 0.134 μs is adopted. Initially, the measured response of time-domain signals from FE simulation for a healthy plate as well as damage plate is shown in Figure 6.18. It is reflected from both the signals that new wave modes are appeared in the signal received from the damaged plate. Another difference between the signals from the healthy and damaged plate is that there is an extraneous mode appearing in the damaged plate.

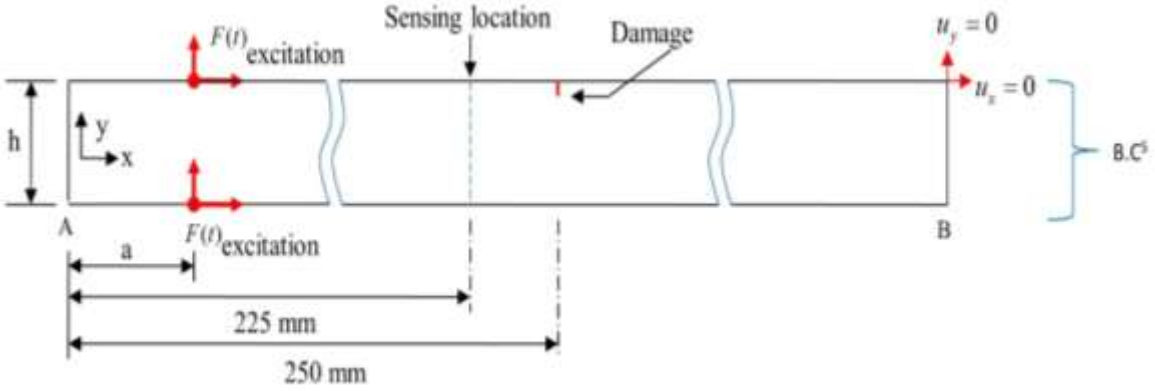

Figure 6. 17. FE model

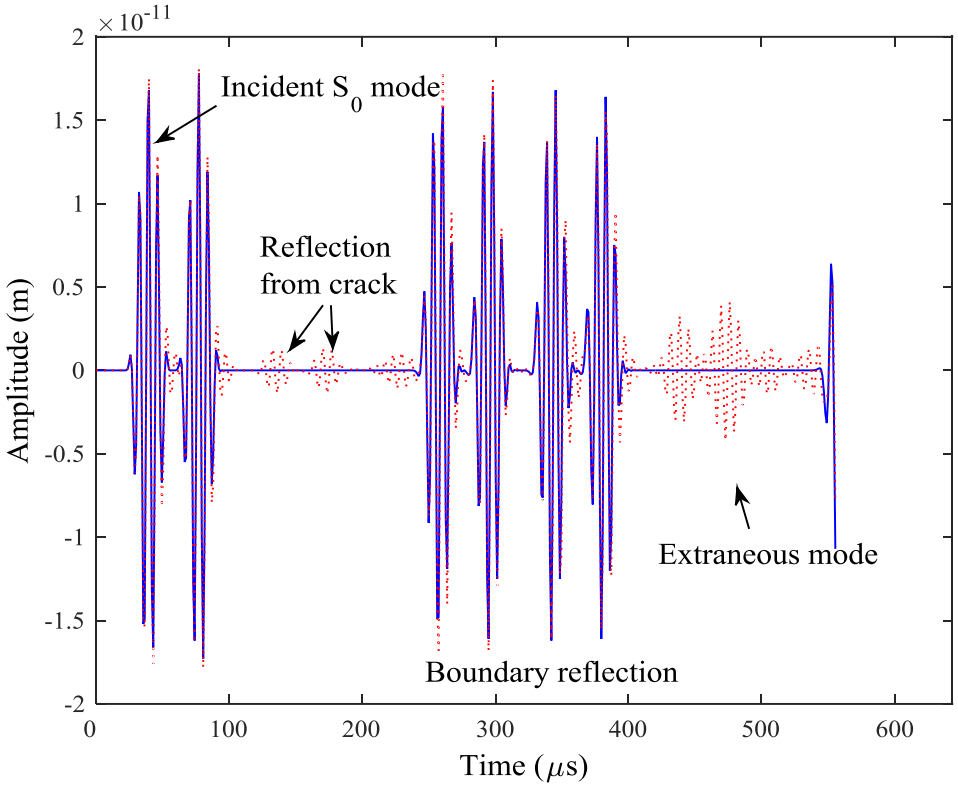

Figure 6.18. Sensor output for S_0 mode excitation for the healthy and damaged plate

(b) Optimal selection of mother wavelet function

In order to decide the optimal wavelet, initially we plot the Shannon's entropy and subsequently the RMSE is compared for various wavelet functions. Figures 6.19-6.20

represent calculated Shannon entropy with respect to transform level for different wavelet functions in case of both the healthy and damage plate signals. It is observed that biorthogonal (bior4.4) represents the lowest trough at transform level 2 in case of DWT based wavelet functions (see Figures 6.19 (a, b)).

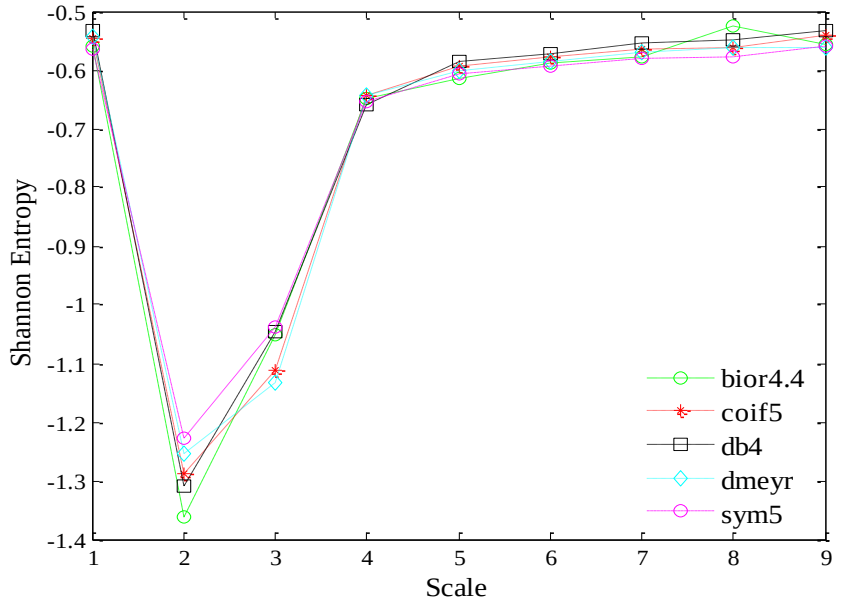

(a) healthy plate

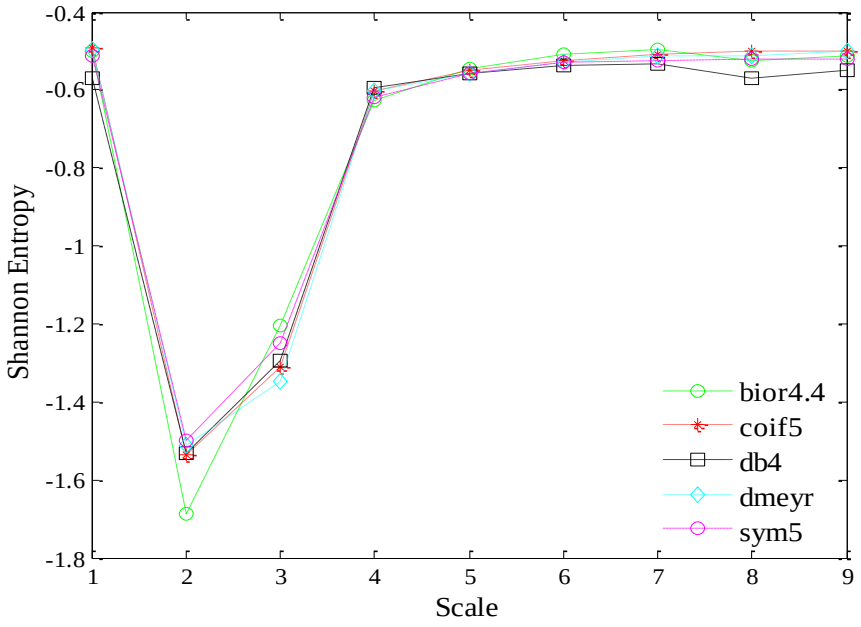

(b) damaged plate

Figure 6.19. Shannon's entropy curves of the DWT from Lamb wave signal

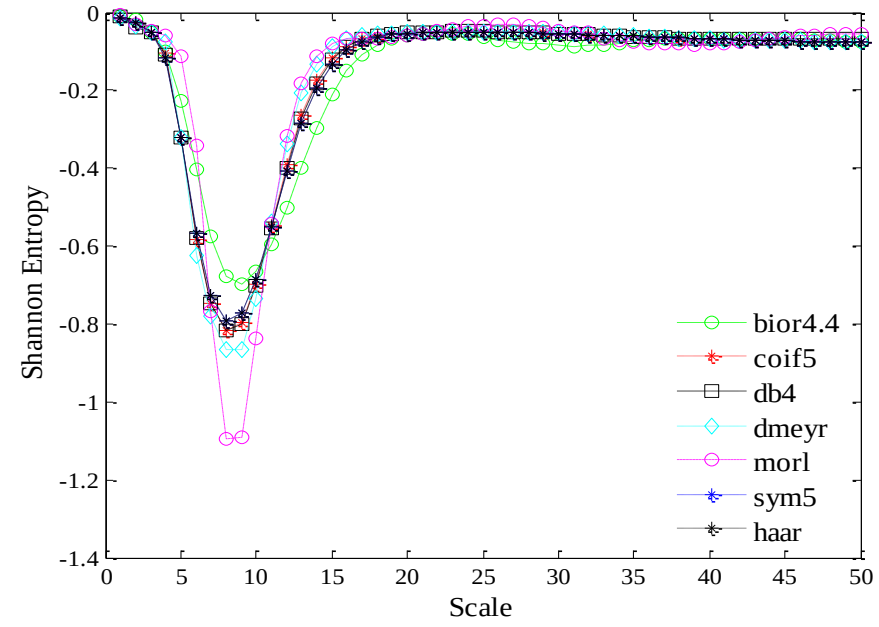

(a) healthy plate.

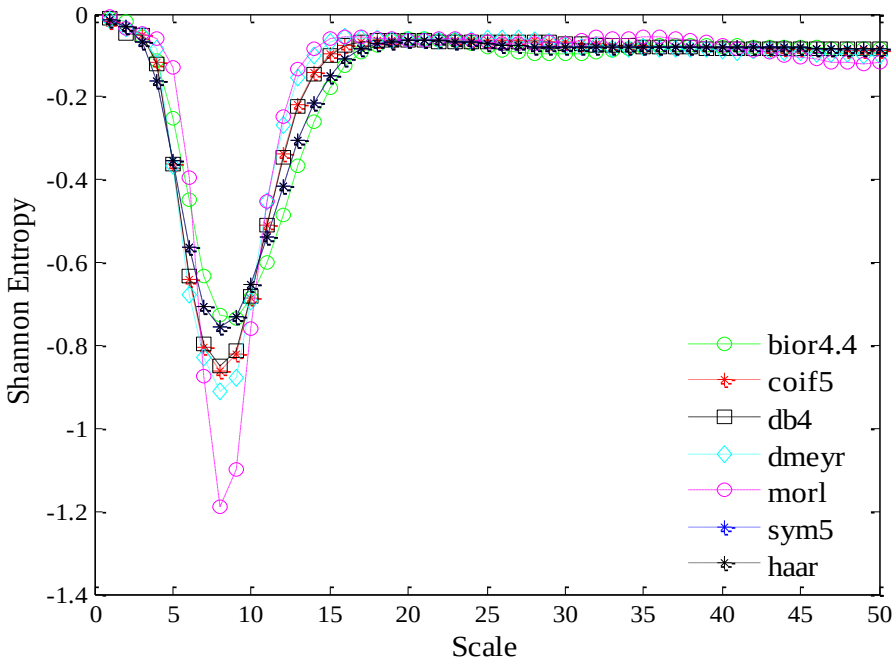

(b) damaged plate.

Figure 6.20. Shannon's entropy curves of the CWT from Lamb wave signal

On the other hand, Morlet wavelet produces the lowest trough at scale level 8 for the CWT based wavelet functions as shown in Figures 6.20(a, b) for both the healthy and damaged plate signals. In order to further test the reliability of the chosen wavelets (bior4.4 and

Morlet) based on Shanon's entropy criterion, RMSE with respect to various SNR values is plotted in Figures 6.21(a-c). It is reflected in Figures 6.21(a, b) based on DWT, that bior4.4 shows the minimum error among the selected wavelet functions.

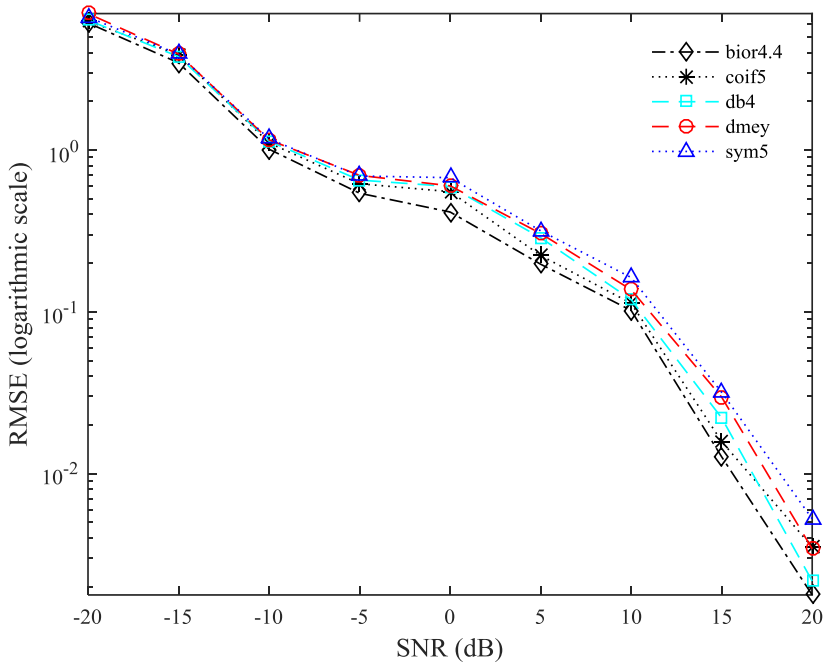

(a) DWT with soft thresholding.

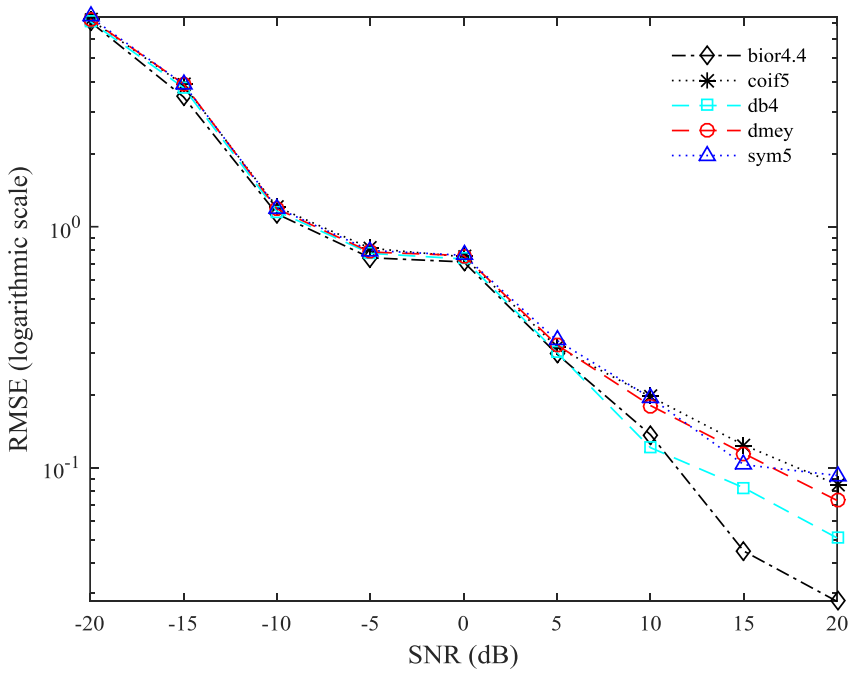

(b) DWT with Hard thresholding.

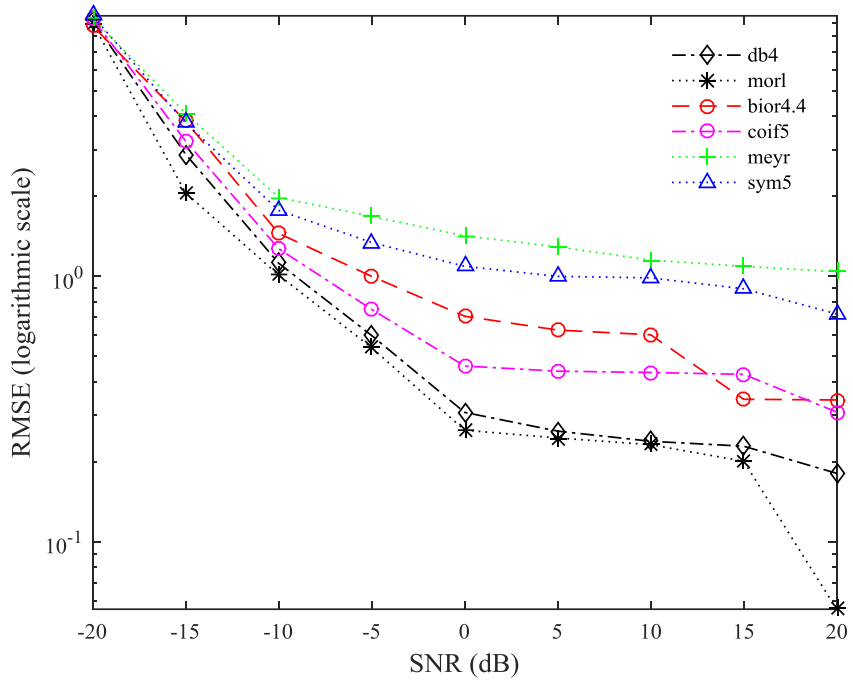

(c) CWT

Figure 6.21. RMSE in various SNR level computed from wavelet transform

In case of CWT based wavelet functions the minimum error is observed in Morlet wavelet as shown in Figure 6.21(c). In all the three cases it is verified that the optimal selection of bior4.4 and Morlet wavelets based on Shannon's entropy criterion is correct.

(c) Denoising and damage detection results using three different filtering techniques

Based on the optimal selection of wavelet, now the performance of the filtering techniques for the damage structure signal is presented. Here, Figure 6.22 represents the contaminated signal of 0 dB from the damage structure whereas Figures (6.23-6.25) describe the filtered signal obtained via the three filtering techniques based on wavelet, matched filter and wavelet matched filter methods, respectively. Figure 6.23 reflects that the wavelet transforms employed are unable to detect properly the signal due to damage in the structure. However, when the same damage structure signal is processed via the MFT the filtered response demonstrates improvement in denoising as compared to the

wavelet transform method as shown in Figure 6.24. Next, the output response as obtained through the use of WMFM is presented in Figure 6.25. It is clear that good response is achieved by proposed technique.

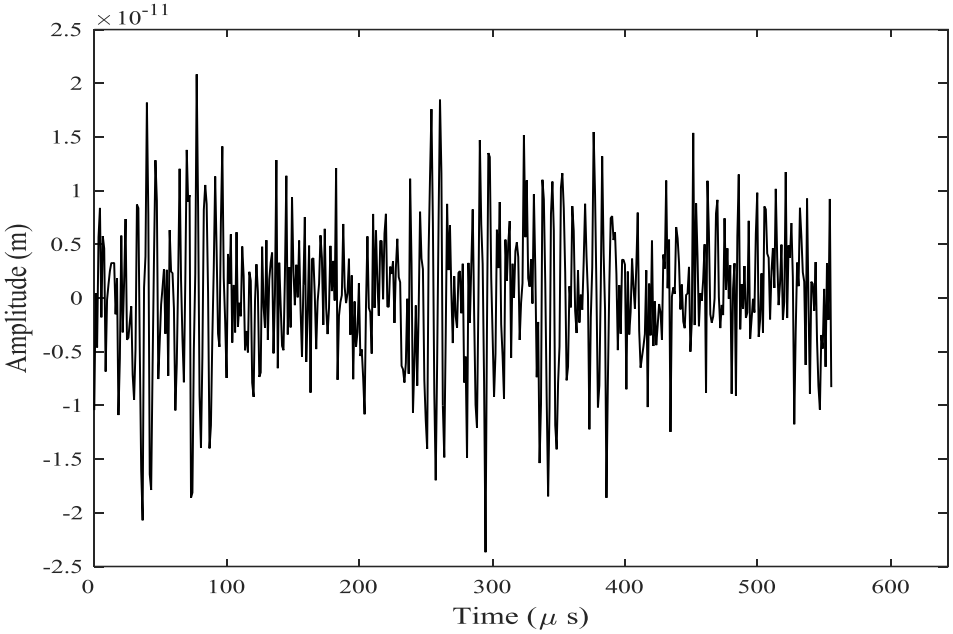

Figure 6.22. A contaminated signal with SNR level 0 dB for damaged plate

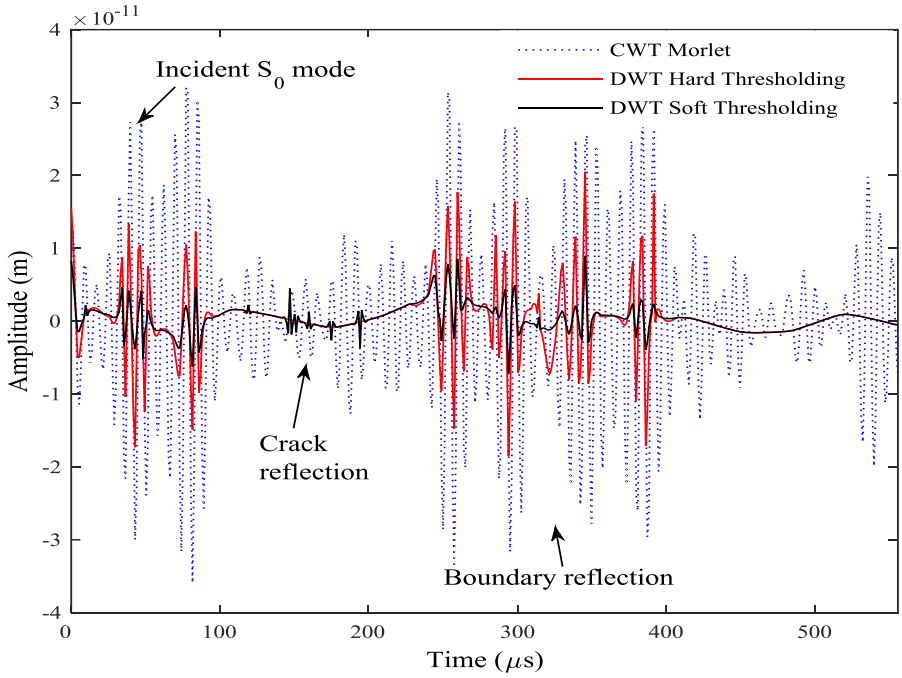

Figure 6.23. Response of wavelet transform for the noisy damaged plate signal with SNR (0 dB)

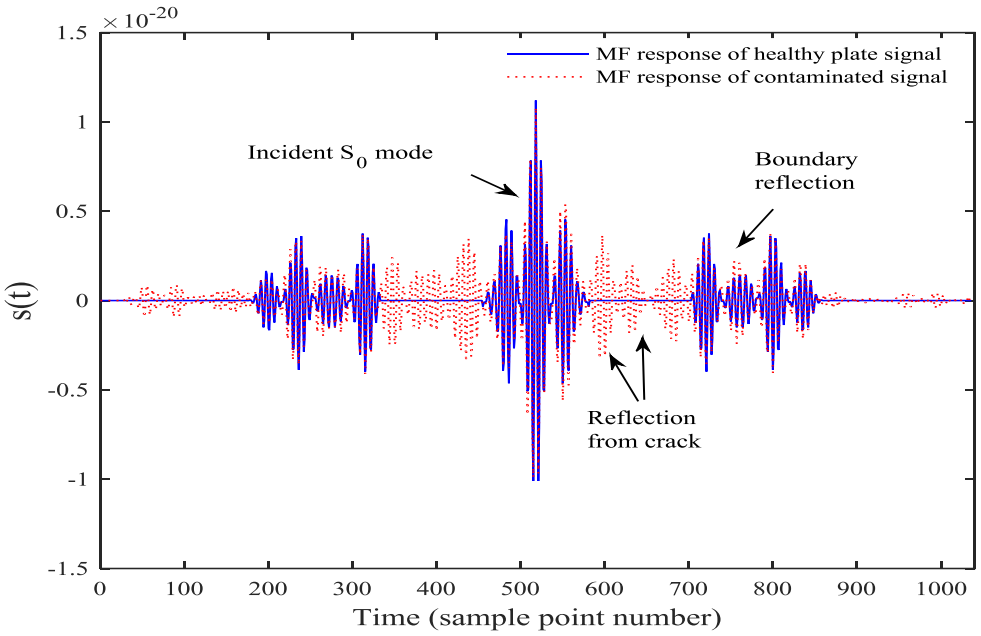

Figure 6.24. MFT response for the noisy signal with SNR (0 dB) convoluted with healthy signal

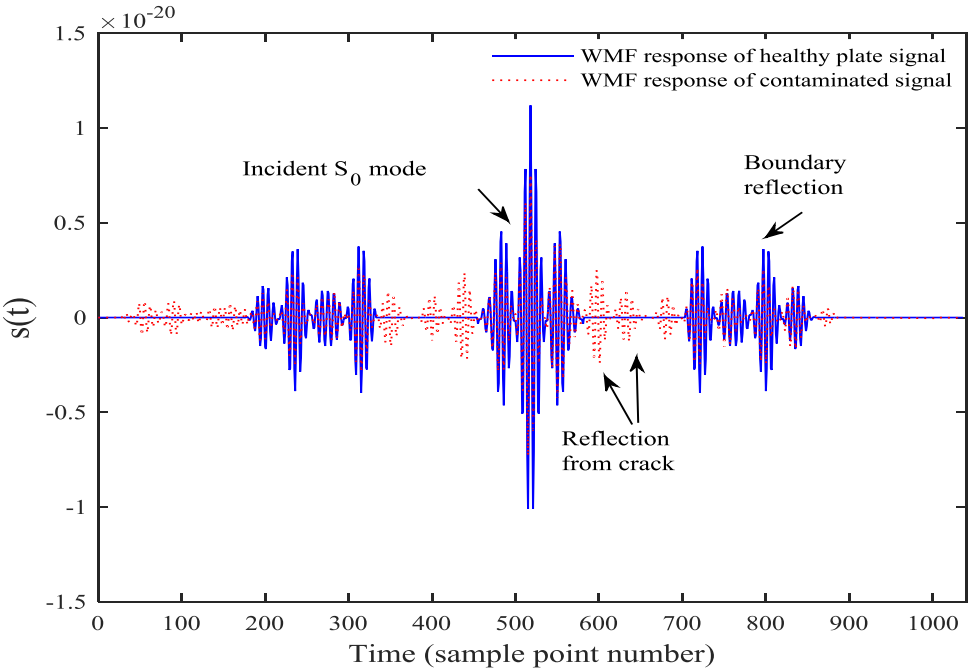

Figure 6.25. The response of WMFM for the noisy damaged plate signal with SNR (0 dB)

The performance of these filtering technique is also evaluated in the presence of coherent noise and shown in Figures (6.26-6.29). Figure 6.26 shows the contaminated

signal with coherent and random noise. In Figure 6.27, denoising is performed using Morlet and DWT based bior4.4 wavelets. This figure reflects that the wavelet transforms are unable to detect damage in the structure.

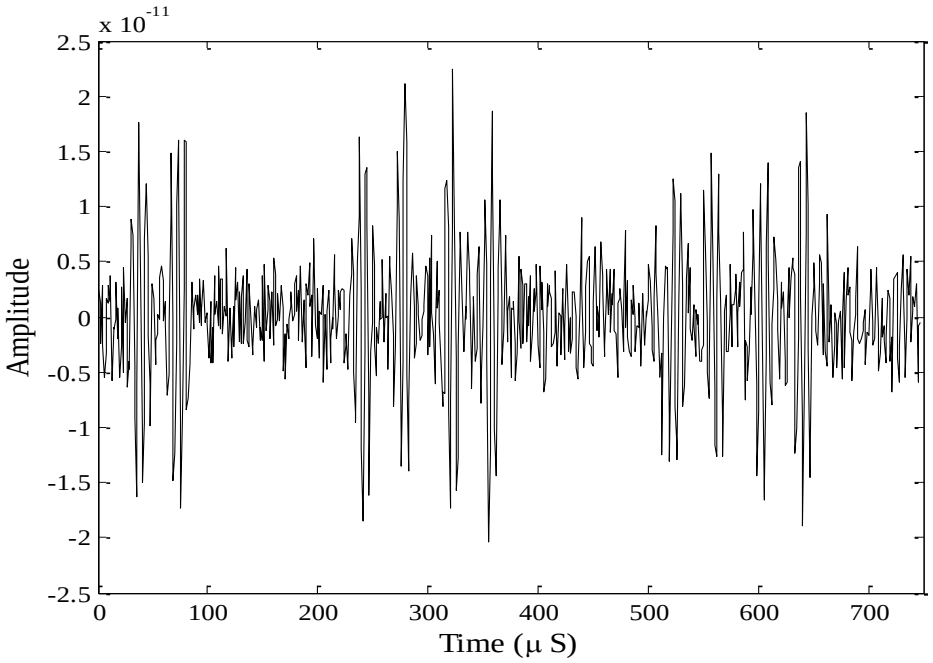

Figure 6.26. A contaminated damaged plate signal with SNR (5 dB) and coherent noise

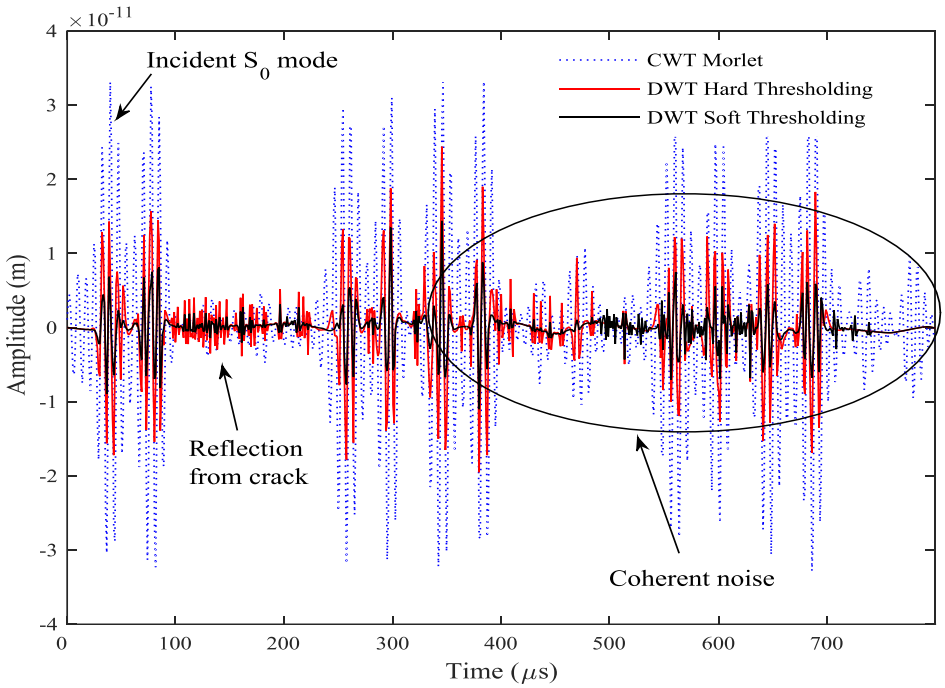

Figure 6.27. Wavelet Transform for the contaminated signal with SNR (5 dB) and coherent noise

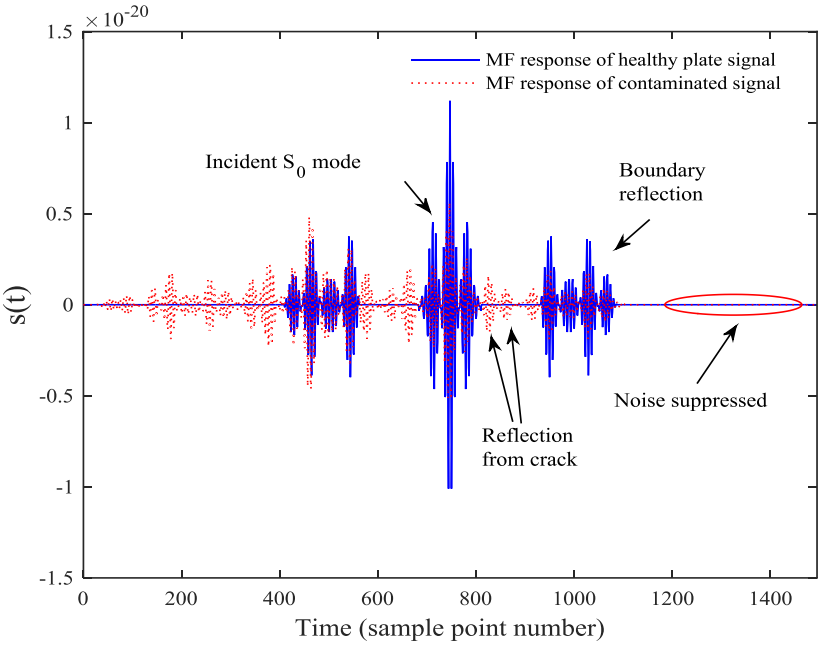

Figure 6.28. MFT response for the contaminated signal with SNR (5 dB) and coherent noise

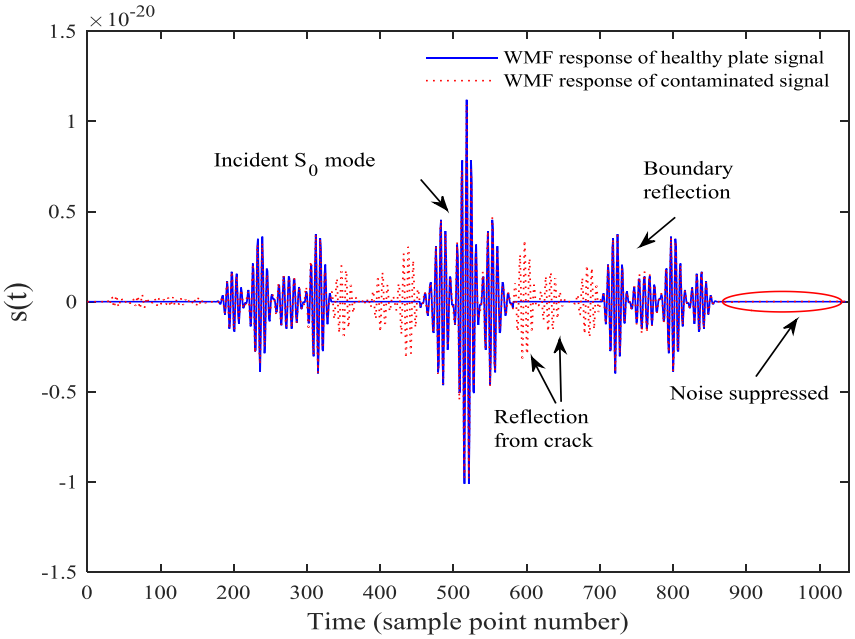

Figure 6.29. The response of WMFM for the contaminated signal with SNR (5 dB)

On the other hand, MFT and WMFM are not only able to remove random noise but also filtering the coherent noise as demonstrated in Figure 6.28 and 6.29. While comparing the responses as obtained by the filtering methods, here, again we can observe that MFT and WMFM help to suppress the noise part to much greater extent and facilitate

to detect the damage easily. It is clear that WMFM have the better capability in noise suppression.

(d) Validation using statistical tools

Table 6.4. Comparison of RMSE, correlation coefficient and post improved SNR of the wavelet based denoising using bior4.4 wavelet function

SNR(dB) (before filtering)	Hard thresholding			Soft thresholding		
	RMSE	Correlation coefficient (*r*)	SNR (dB) (after filtering)	RMSE	Correlation coefficient (*r*)	SNR(dB) (after filtering)
20	0.0278	0.9887	31.16	0.0185	0.9898	34.28
15	0.045	0.9801	27.58	0.0424	0.9865	31.15
10	0.137	0.9713	21.97	0.097	0.9801	23.79
5	0.306	0.9629	16.69	0.256	0.9759	17.41
0	0.754	0.9495	7.87	0.55	0.9523	10.63
-5	0.743	0.7626	3.13	0.714	0.8027	4.52
-10	1.13	0.6352	-2.859	0.909	0.7015	0.12
-15	3.96	0.197	-8.46	3.88	0.3628	-7.1
-20	7.1	0.1031	-13.57	7.26	0.1082	-11.89

The similar studies are carried out as explained in the earlier section. The correlation coefficient of the final signal with respect to noise free signal for all the three methods is presented in Tables (6.4-6.6). Table 6.4 presents the calculated correlation coefficients and RMSE values for the wavelet-based hard and soft thresholding methods. It can be observed that denoising results are acceptable according to estimated value of the correlation coefficient. Table 6.5 is constructed for matched filtering technique in order to evaluate denoising ability with various SNR and it is evident that the proposed matched filtering method is performing well in comparison with wavelet based denoising.

Table 6.6 provides comparison of the wavelet matched filter method with the hard and soft thresholding. Again, it is reflected from the Tables (6.4-6.6), the proposed WMFM technique works very well.

Table 6.5. Comparison of RMSE, correlation coefficient and post improved SNR of the MFT

SNR(dB) (before filtering)	Matched filtering technique		
	MSE	Correlation coefficient (*r*)	SNR (dB) (after filtering)
20	0.00658	0.9891	35.34
15	0.0244	0.9875	31.05
10	0.0674	0.9781	24.79
5	0.178	0.9768	17.97
0	0.438	0.9613	11.73
-5	0.686	0.8492	7.9
-10	0.888	0.7314	0.12
-15	3.75	0.4623	-3.4
-20	6.54	0.2175	-9.71

Table 6.6. Comparison of RMSE, correlation coefficient and post improved SNR of the WMFM using bior4.4 wavelet function

SNR(dB) (before filtering)	Wavelet matched filter method					
	Hard thresholding			Soft thresholding		
	MSE	Correlation coefficient (*r*)	SNR(dB) (after filtering)	MSE	Correlation coefficient (*r*)	SNR(dB) (after filtering)
20	0.00606	0.9889	36.27	0.00665	0.9899	37.12
15	0.0206	0.9815	32.75	0.0173	0.9877	34.95
10	0.0531	0.9781	25.83	0.0428	0.9851	26.19
5	0.118	0.9759	19.41	0.103	0.9789	22.17
0	0.398	0.9613	12.73	0.327	0.97	14.61
-5	0.517	0.8547	8.12	0.509	0.8747	9.83
-10	0.888	0.7615	1.12	0.752	0.7729	2.47
-15	3.13	0.4826	-2.8	1.97	0.4896	-2.12
-20	6.01	0.2982	-8.53	5.91	0.3092	-8.19

6.2 Modeling of Lamb Wave for Cylindrical Structures

Shell type structures like thin walled tubes and hollow cylinders are widely used in oil, gas and chemical industries. Lamb wave inspection systems not only offer the capability for identification of flaws of long pipe works but also extend great potential for switching from schedule based maintenance to conditioned-based maintenance (Alleyne *et al.* (2000), Zhu (2002), Wang *et al.* (2015)). Many theoretical and experimental investigations have shown the excellent possibility in the application of guided wave propagation techniques applicable to pipes (Demma *et al.* (2003), Vogelaar and Golombok (2016), Duan *et al.* (2016)). The objective of this section is to establish the effective multi-feature techniques of signal analysis for problems of guided wave based structural health monitoring in cylindrical shell structures. The interaction of Lamb waves with circumferential defects is examined by using this technique.

(a) Finite element simulation

Three dimensional FE model of a hollow cylinder is considered in the present analysis and simulated using the commercial FEM software ABAQUS for the Lamb wave propagation as shown in Figure 6.30. The position of a sensing point and notch are demonstrated in the same figure. To compute the responses of Lamb wave interaction under excitation frequencies 50 kHz, FE modal is excited by imposing a time-varying pin force in the 'in-phase' along the longitudinal (propagating) direction. Force on left part of the pipe as shown in Figure 6.30 is applied on all circumferential nodes of the left edge of the hollow cylinder to generate the longitudinal L (0,2) Lamb wave mode. The transverse T (0,1) Lamb wave mode are propagated by imposing, out-of-phase pin forces parallel to the circumferential direction. A brass pipe of 1000 mm length, 30 mm inner diameter and 10 mm wall thickness is considered in present analysis. The material

properties of brass assumed are Poisson's ratio 0.324; density 8400 Kg/m^3; Young's modulus 106 GPa. Hollow cylinder with and without defect of notch is discretized using ten-node tetrahedral element of ABAQUS (C3D10). The initial simulation is performed for a healthy brass hollow cylinder. Next simulation is carried out on the brass hollow cylinder with 360^0 circumferential notch of 4 mm width and 2.5 mm depth. Typical snapshots of Lamb wave propagation and scattering induced by circumferential notch and boundary in the damaged cylinder with different times frame are demonstrated in Figure 6.31. The measured response of time-domain signals from FE simulation for a healthy cylinder as well as damage cylinder is shown in Figure 6.32. It is reflected from the comparison of healthy and damaged cylinder signals that new wave packets are appeared in the signal received from the damaged hollow cylinder. Damage is observed by analyzing echoes in the received response due to wave reflections away from damaged regions.

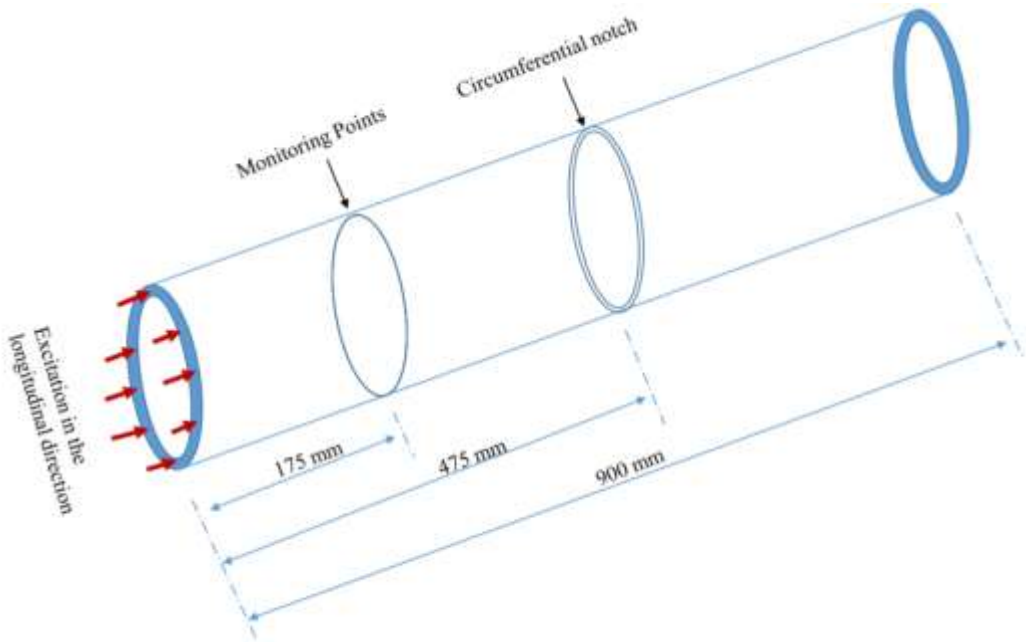

Figure 6.30. The configuration of a hollow cylinder with circumferential notch

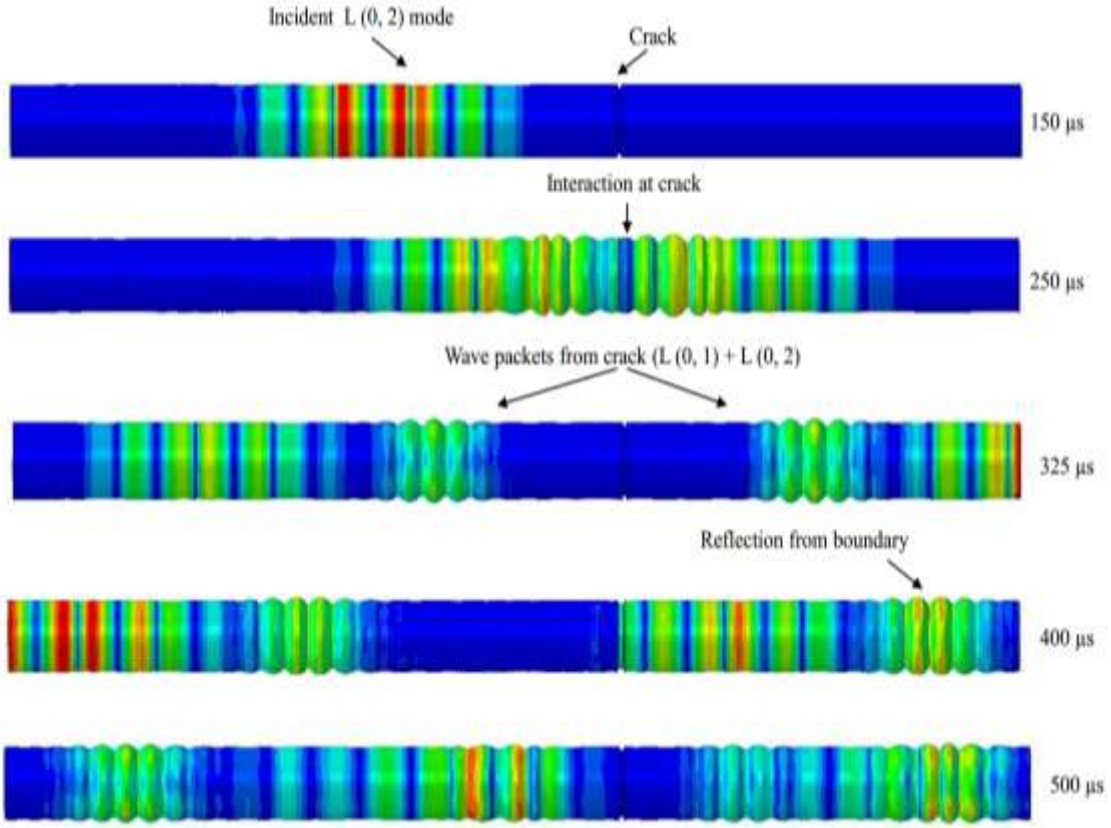

Figure 6.31. Snapshots of FE Simulation of Lamb wave propagation in brass pipe and scattering

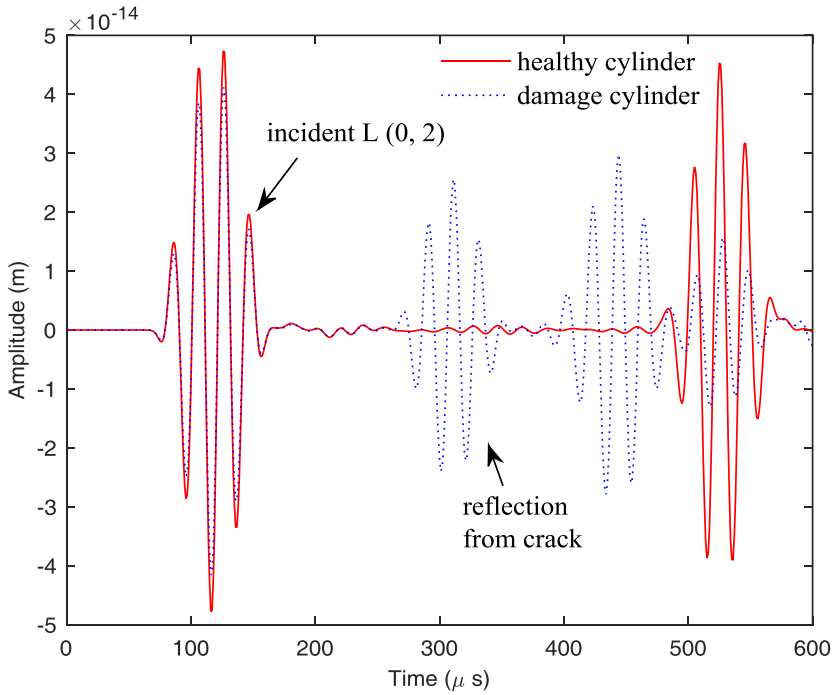

Figure 6.32. Sensor output for the L (0, 2) mode excitation for healthy and damaged cylinder

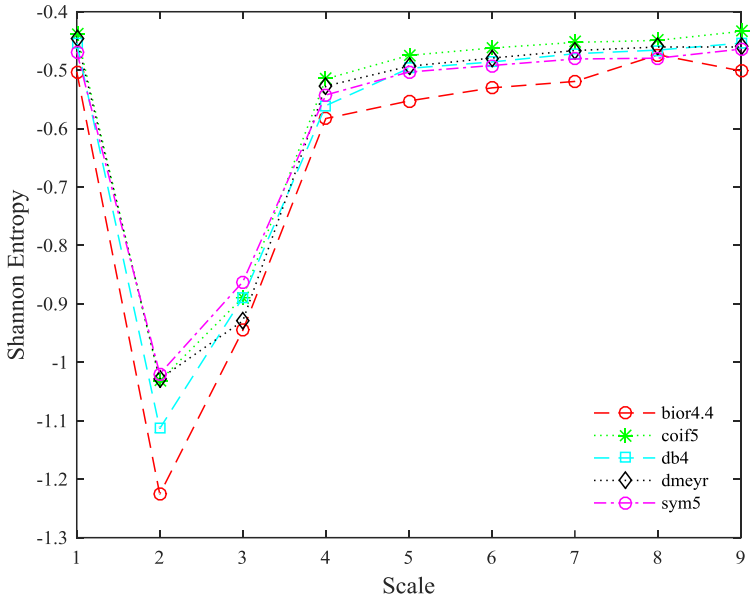

(a) healthy cylinder

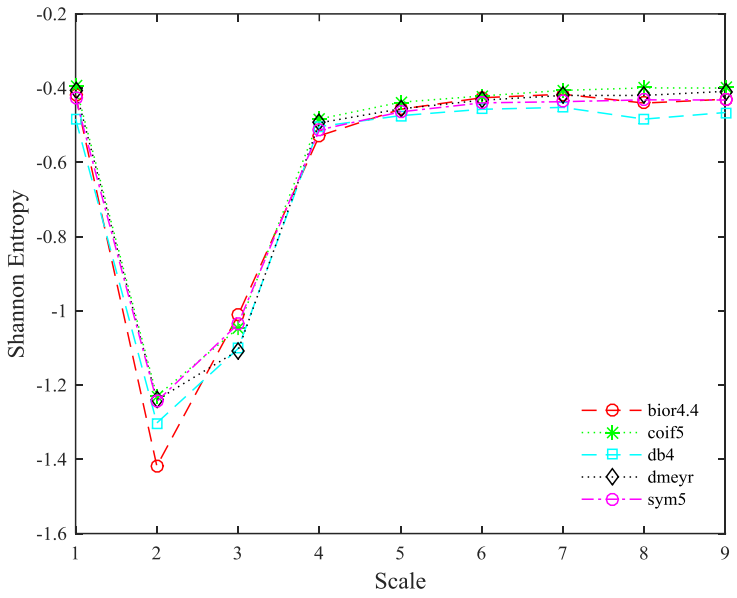

(b) damaged cylinder

Figure 6.33. Shannon's entropy curves of the DWT from Lamb wave signal

(b) Optimal selection of mother wavelet function

Figures 6.33-6.34 represent calculated Shannon entropy with respect to transform level for different wavelet functions based on DWT and CWT in case of both the healthy and damage cylinder signals. Figures 6.33(a, b) illustrate Shannon's entropy in case of

DWT based wavelet for both healthy and damaged cylinder signals. It is found that biorthogonal (bior4.4) shows the lowest trough at transform level 2. On the other hand, Morlet wavelet represents the lowest trough at scale level 8 for the CWT based wavelet functions as shown in Figures 6.34 (a, b). To further examine the reliability of the chosen wavelets, we follow the RMSE with respect to various SNR values, Figures 6.35(a-b) based on soft and hard thresholding, respectively show that bior4.4 delivers the minimum error among the selected wavelet functions. For CWT based wavelet functions the minimum error is obtained in Morlet wavelet as depicted in Figure 6.35(c).

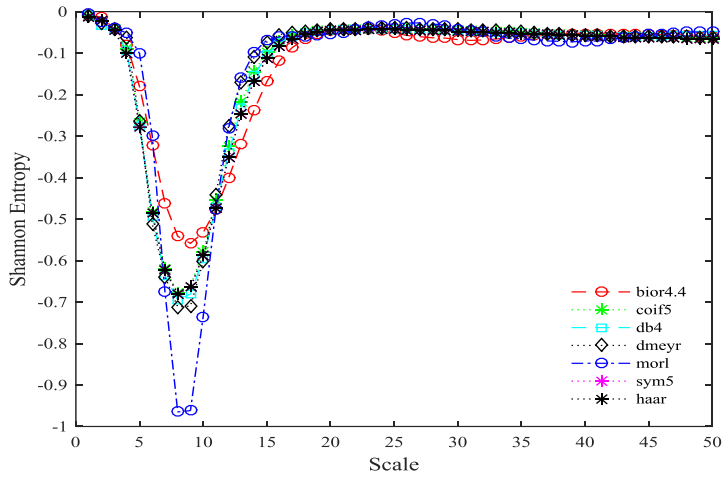

(a) healthy cylinder

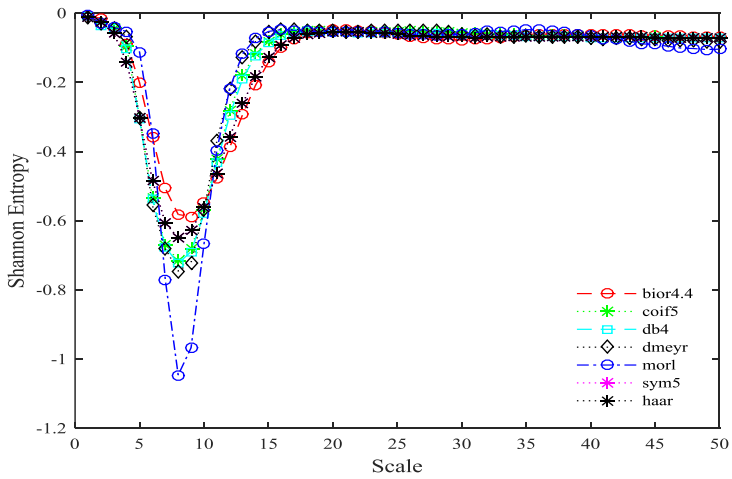

(b) damaged cylinder

Figure 6.34. Shannon's entropy curves of the CWT from Lamb wave signal

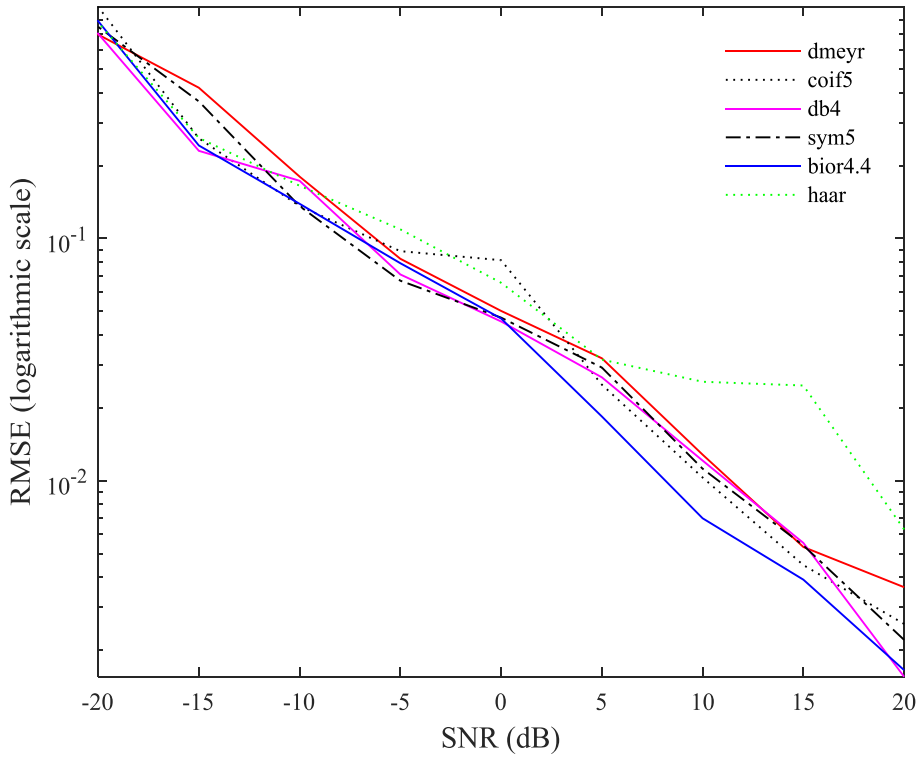

(a) DWT with soft thresholding

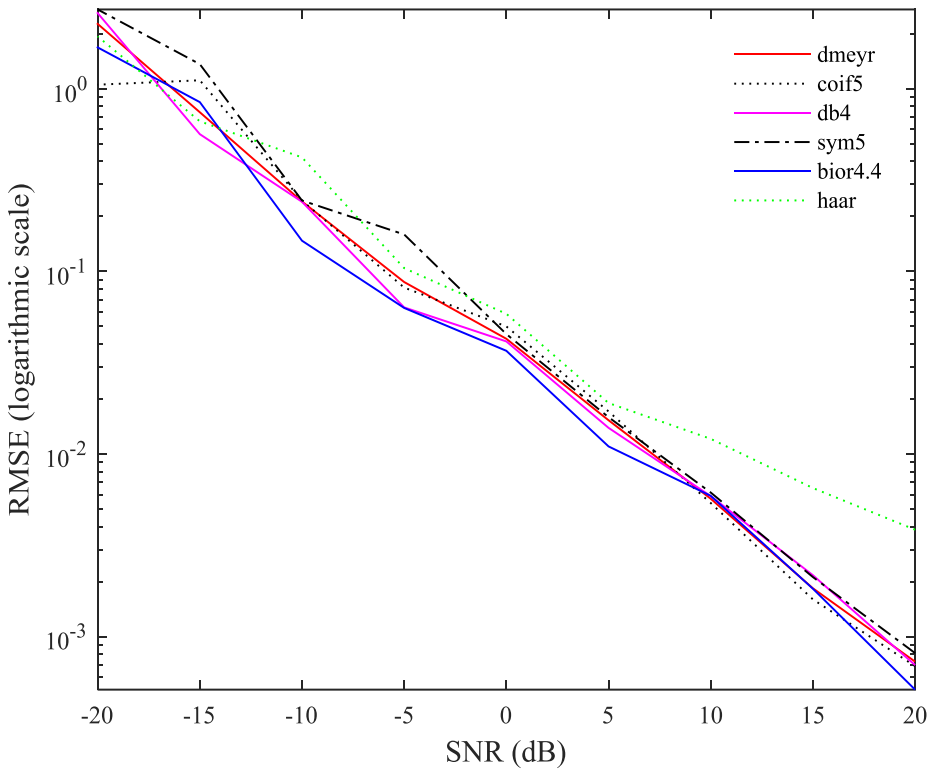

(b) DWT with Hard thresholding

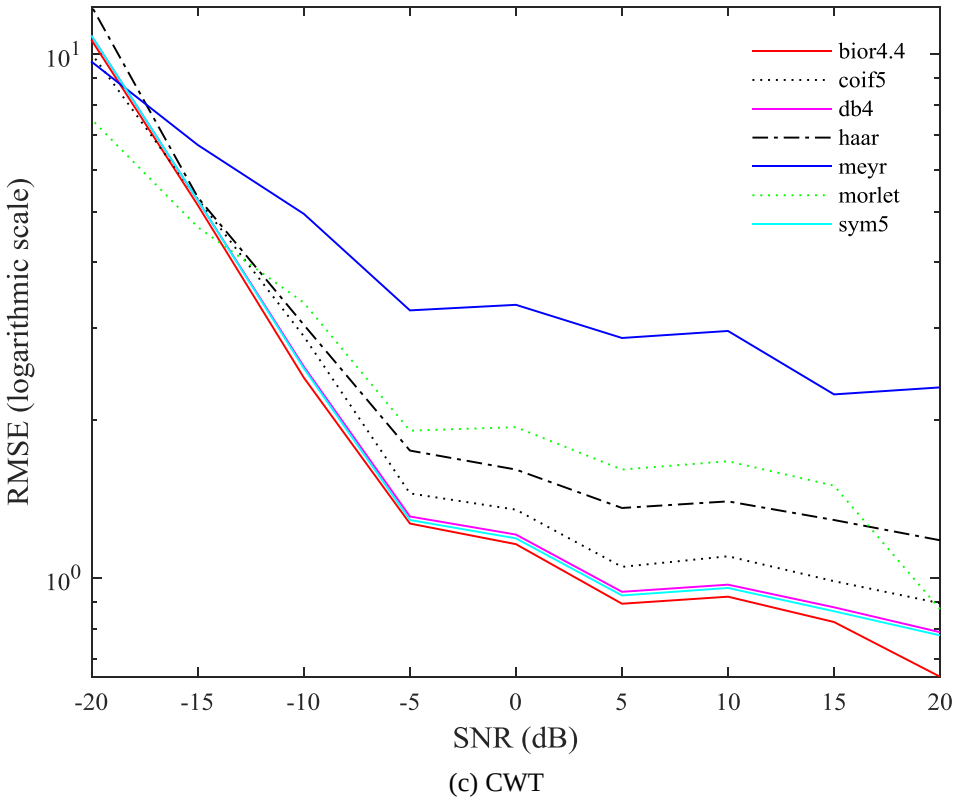

Figure 6.35. RMSE in various SNR level computed from wavelet transform

(c) Denoising and damage detection results using three different filtering techniques

Figure 6.36 shows the noisy signal of 0 dB from the damage structure whereas Figures (6.37-6.39) describe the filtered signal obtained through filtering methods. It is clear from Figure 6.36 that original signal from the damage structure is lost in the noise. In Figure 6.37, denoising is performed using CWT based Morlet and DWT based bior4.4 wavelets. This figure represents that the wavelet transforms are unable to detect damage in the structure. However, when the same damage cylinder signal is processed by the MFT the filtered response reflects enhancement in denoising as compared to the wavelet transform (see Figure 6.38). However, some unwanted wave packets are visible in the final output signal. In Figure 6.39, we plot the output response received through the use of WMFM. We can observe that WMFM help to suppress the noise and facilitate to detect

the damage easily. The performance of these filtering technique is also evaluated in the presence of coherent noise and shown in Figures (6.40-6.43). Figure 6.40 shows the contaminated signal with coherent and random noise.

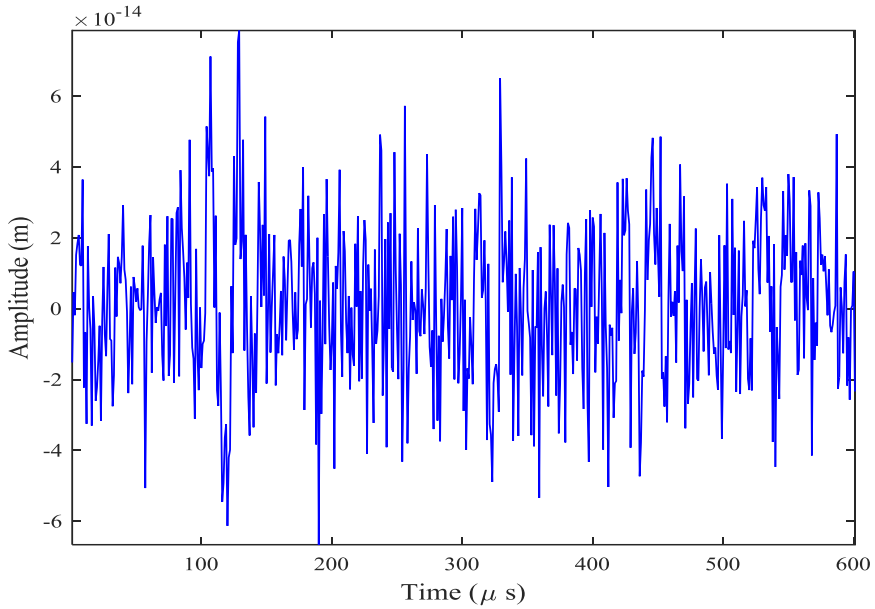

Figure 6.36. A contaminated signal with SNR (0 dB) for damaged cylinder

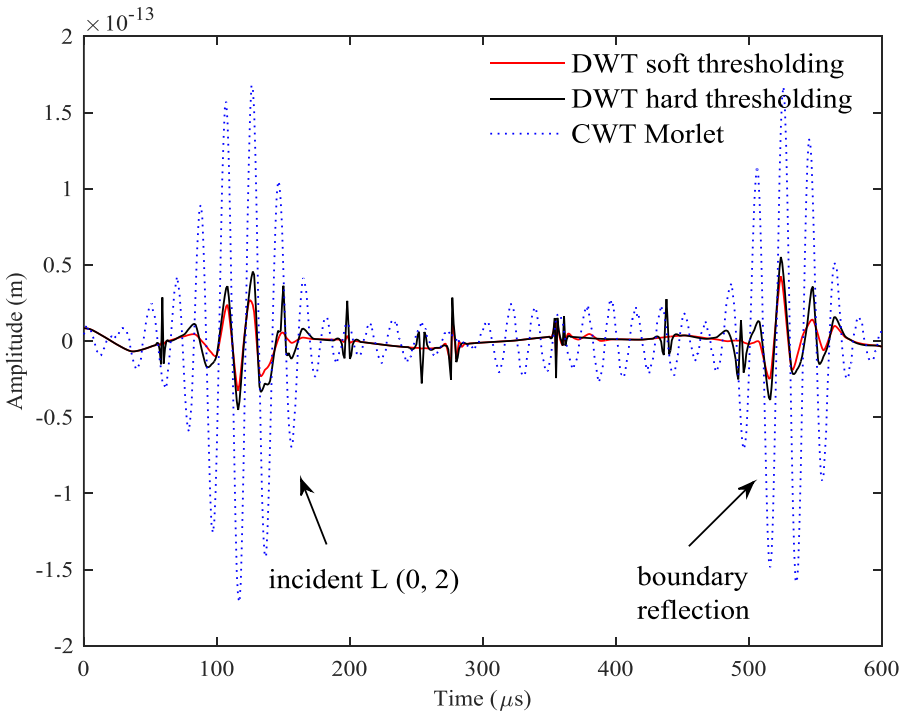

Figure 6.37. Response of wavelet transform for the noisy damaged cylinder signal with SNR (0 dB)

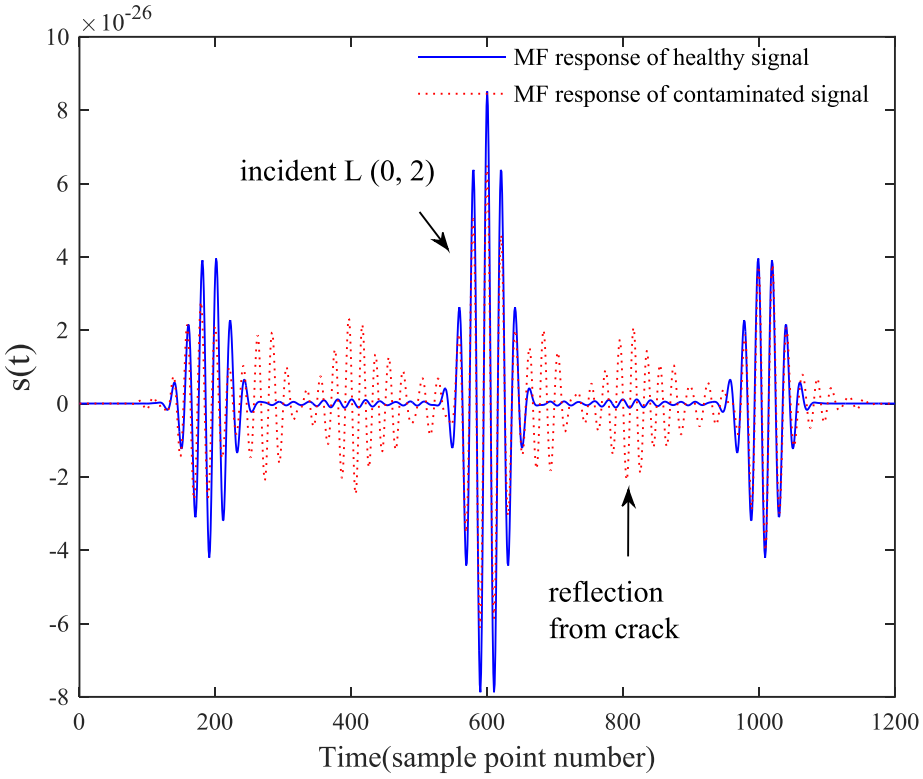

Figure 6.38. MFT response for the noisy signal with SNR (0 dB) convoluted with healthy signal

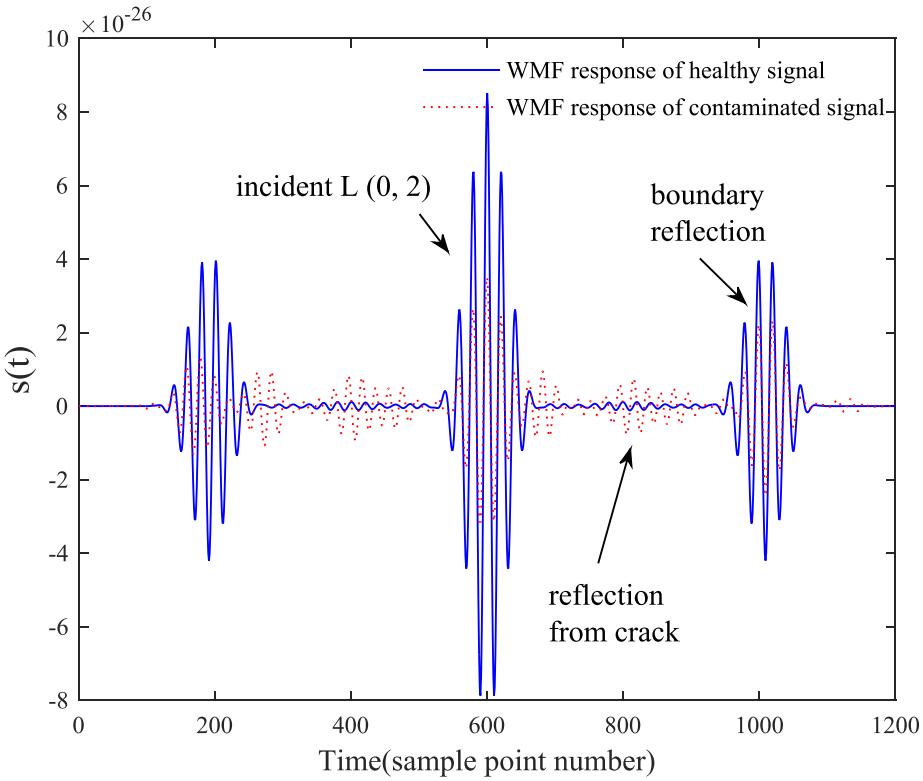

Figure 6.39. The response of WMFM for the noisy damaged cylinder signal with SNR (0 dB)

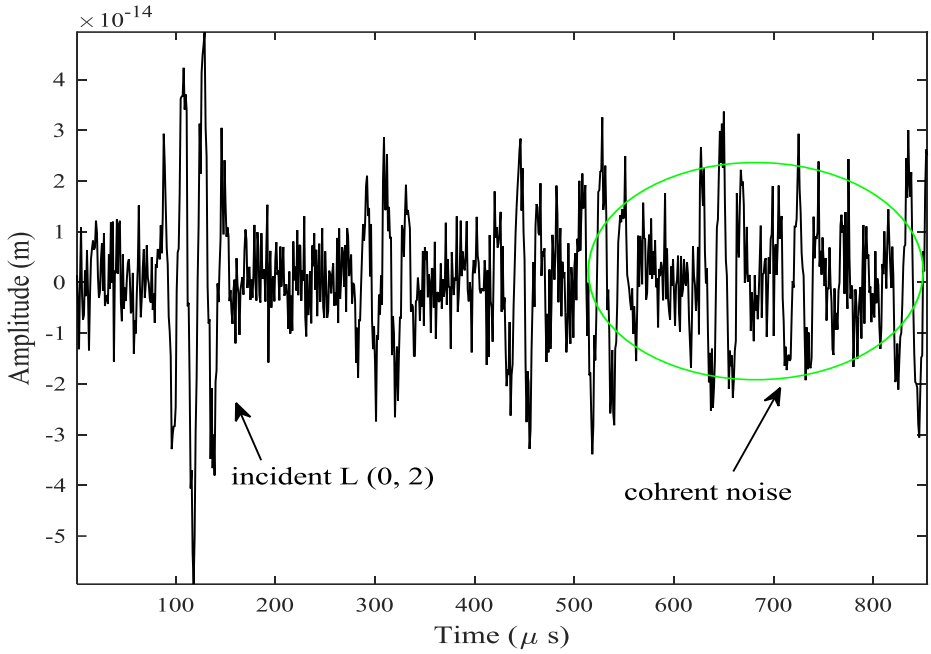

Figure 6.40. A contaminated damaged cylinder signal with SNR (5 dB) and coherent noise

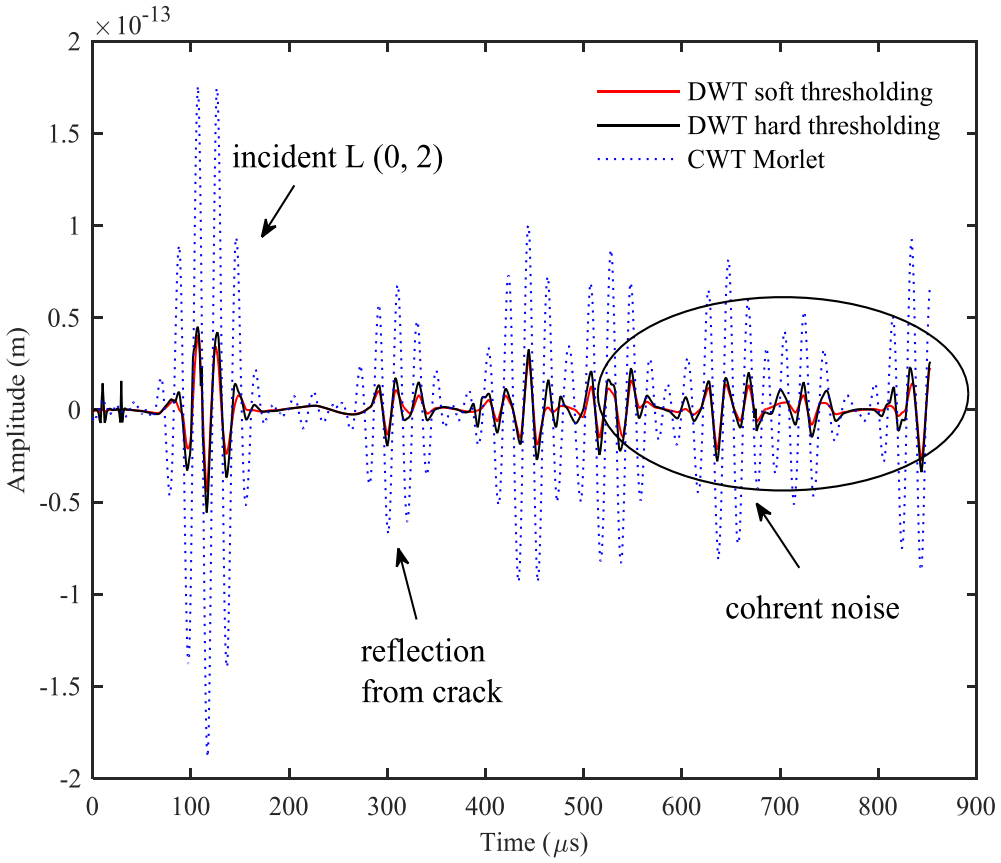

Figure 6.41. Wavelet Transform for the contaminated signal with SNR (5 dB) and coherent noise

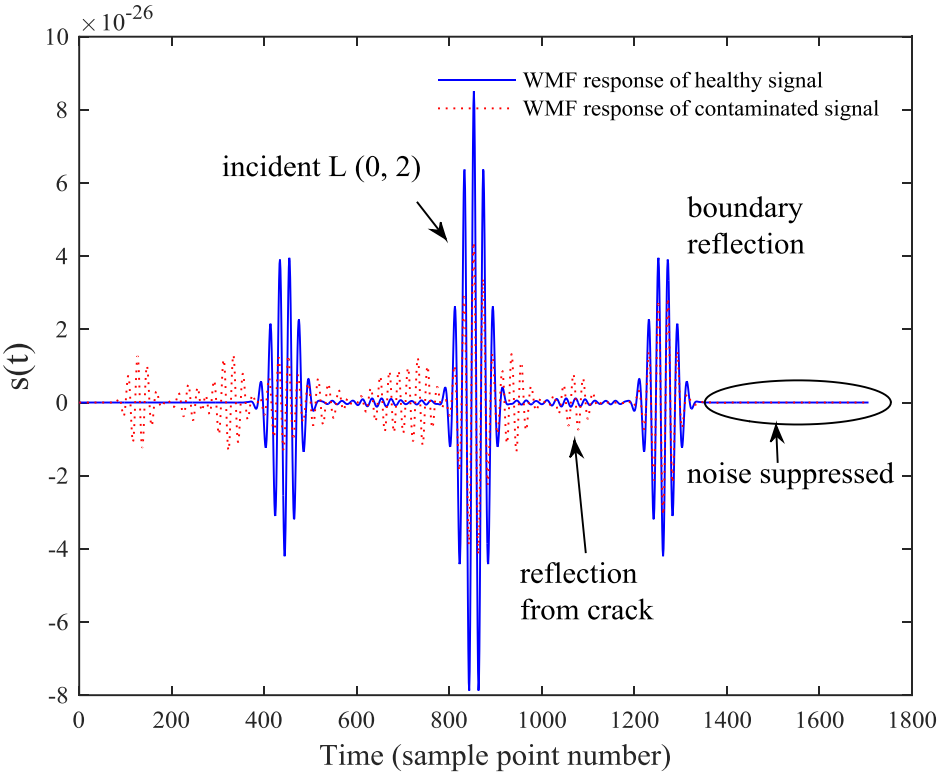

Figure 6.42. MFT response for the contaminated signal with SNR (5 dB) and coherent noise

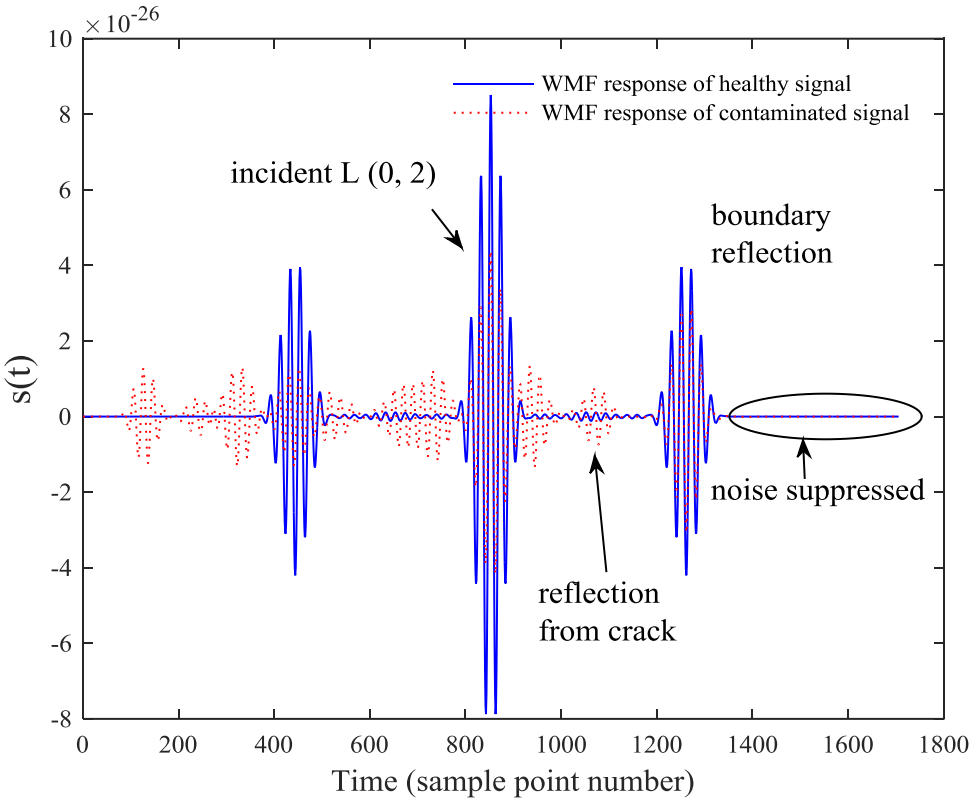

Figure 6.43. The response of WMFM for the contaminated signal with SNR 5 dB

In Figure 6.41, denoising is performed using Morlet and DWT based bior4.4 wavelets. This figure shows that the wavelet transforms are unable to detect damage in the structure. On the other hand, MFT and WMFM are not only able to remove random noise but also filtering the coherent noise as demonstrated in Figure 6.42 and 6.43.

Table 6.7. Comparison of RMSE, correlation coefficient and post improved SNR of the wavelet based denoising for various SNR using bior4.4 wavelet function

SNR(dB) (before filtering)	Hard thresholding			Soft thresholding		
	RMSE	Correlation coefficient (*r*)	SNR (dB) (after filtering)	RMSE	Correlation coefficient (*r*)	SNR(dB) (after filtering)
20	0.0267	0.9886	32.21	0.0187	0.9897	33.78
15	0.045	0.9805	27.68	0.0436	0.9867	30.15
10	0.138	0.9723	22.87	0.0961	0.9814	24.97
5	0.316	0.9638	16.79	0.258	0.9795	18.41
0	0.762	0.9483	7.86	0.658	0.9153	11.02
-5	0.753	0.7646	3.43	0.726	0.8072	4.12
-10	1.22	0.6361	-2.659	0.908	0.7114	0.12
-15	3.98	0.198	-8.14	3.87	0.3521	-7.25
-20	7.85	0.1045	-13.28	7.15	0.1072	-11.98

To compare the efficiency of the proposed filtering techniques we demonstrate here the correlation coefficient of the processed signal with respect to noise free signal for all the three methods, Tables (6.7-6.9). Table 6.7 presents the calculated correlation coefficients and RMSE values for the wavelet-based hard and soft thresholding methods. It can be observed that denoising results are acceptable according to estimated value of the correlation coefficient. Table 6.8 shows the performance of MFT in order to evaluate denoising ability. It is evident that the proposed matched filtering method is performing well in comparison with wavelet based denoising. Table 6.9 provides comparison of the WMFM with the hard and soft thresholding. Finally, from all the three tables and

comparing the correlation coefficient, RMSE and SNR values of filtered signal, it establishes that the new concept of WMFM may be a very suitable noise filtering method.

Table 6.8. Comparison of RMSE, correlation coefficient and post improved SNR of the matched filtering technique for various SNR

SNR(dB) (before filtering)	Matched filtering technique		
	MSE	Correlation coefficient (*r*)	SNR (dB) (after filtering)
20	0.00569	0.9890	35.14
15	0.0214	0.9878	30.24
10	0.0664	0.9788	24.69
5	0.179	0.9758	16.98
0	0.336	0.9602	10.83
-5	0.676	0.8482	6.08
-10	0.928	0.7228	0.03
-15	4.052	0.4618	-3.02
-20	7.508	0.2267	-9.68

Table 6.9. Comparison of RMSE, correlation coefficient and post improved SNR of the wavelet matched filter technique for various SNR using bior4.4 wavelet function

SNR(dB) (before filtering)	Wavelet matched filter method					
	Hard thresholding			Soft thresholding		
	MSE	Correlation coefficient (*r*)	SNR(dB) (after filtering)	MSE	Correlation coefficient (*r*)	SNR(dB) (after filtering)
20	0.00616	0.9890	36.18	0.00658	0.9898	37.24
15	0.0228	0.9826	31.76	0.0175	0.9876	33.12
10	0.0584	0.9782	24.98	0.0446	0.9865	26.02
5	0.146	0.9748	18.44	0.115	0.9778	21.12
0	0.386	0.9634	11.73	0.338	0.9706	13.78
-5	0.548	0.8536	7.24	0.514	0.8738	8.18
-10	0.879	0.7502	0.26	0.772	0.7626	1.69
-15	3.352	0.4832	-3.98	1.872	0.4886	-2.46
-20	5.184	0.2976	-8.45	4.176	0.3084	-8.28